A new neuromuscular driver model for steering system development

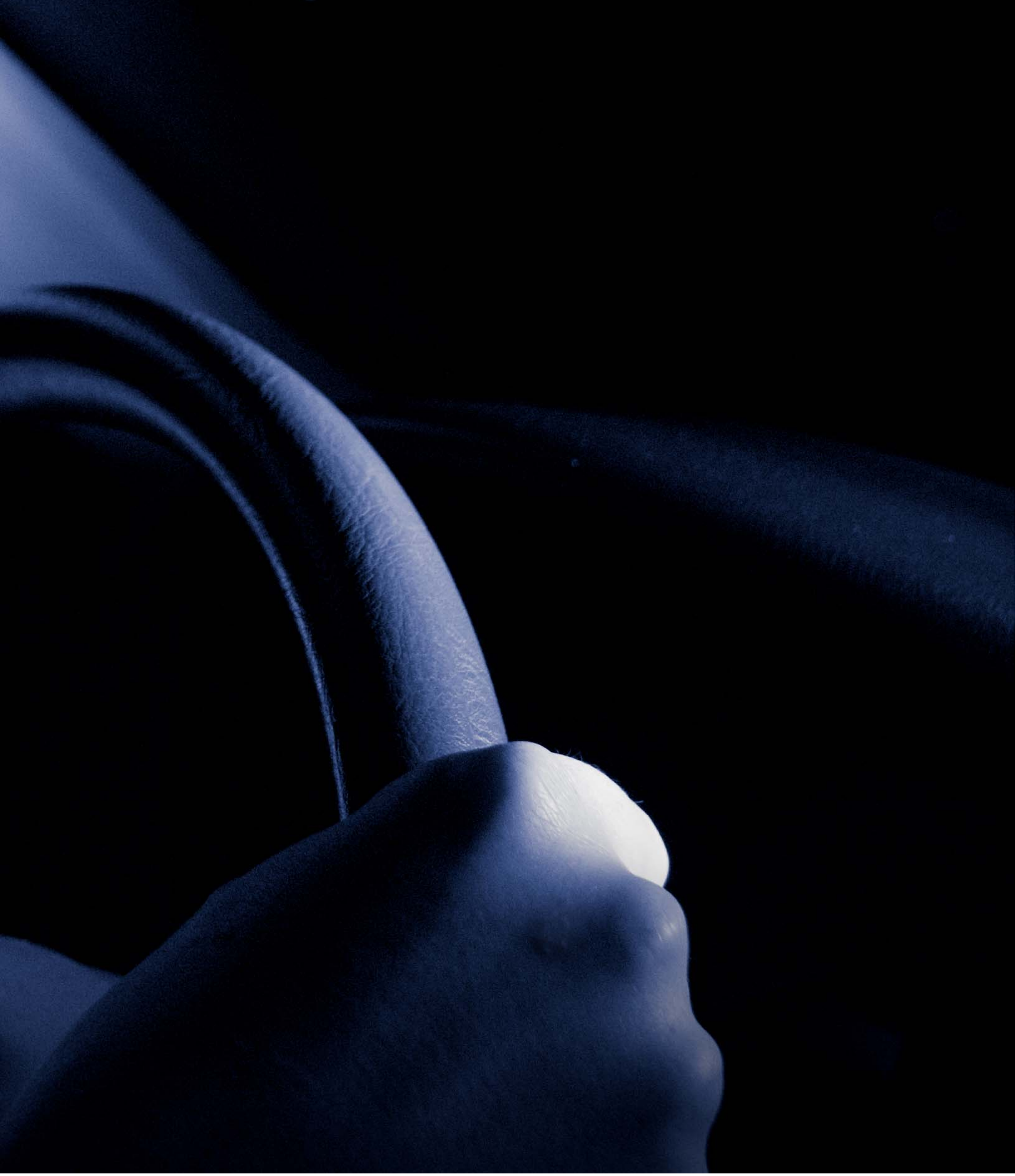

A new neuromuscular driver model for steering system development

Master Thesis Report as part of the Master Mechanical Engineering, track Biomechanical Design, specialization Automotive

Cas Droogendijk
Wb 1107259

5 April 2010

Supervisors:

Prof. dr. ir. E.G.M. Holweg	E.G.M.Holweg@tudelft.nl
Dr. ir. R. Happee	R.Happee@tudelft.nl
Dr. ir. D.A. Abbink	D.A.Abbink@tudelft.nl
D. Katzourakis MSc	D.Katzourakis@tudelft.nl

Faculty of Mechanical, Maritime and Materials Engineering (3ME)
BioMechanical Engineering
Delft University of Technology
Mekelweg 2, 2628 CD Delft, the Netherlands

1. Abstract

Designing steering systems which improve safety and comfort requires focus on the needs, wants and limitations of the driver, which in industry are defined by a certain "steering feel". Many different steering feels have been proposed over the past decades, each describing the optimal relation between the torque applied on the steering wheel and the resulting steering wheel angle. As a result, traditional design methods rely heavily on evaluation with real cars or with driving simulators by expert drivers. This is a time consuming trial and error process, based on subjective driver opinions. Substituting the driver by a driver model can improve this evaluation method, and enables us to get insight into the poorly understood human driving behavior. If both vehicle and driver are replaced by a computer model, computerized optimization routines can be implemented to find the optimal steering system design.

The requirements on the driver model necessitated the development of a new driver model, which is based on two models. A conventional preview driver model, which lacks the modeling of physical limitations and the response to steering torque feedback, and a neuromuscular driver model, which is limited to describing feedback behavior in a single operating point. Two major model adjustments over the original neuromuscular model were implemented to make the realized angle follow the desired angle without being constrained to a fixed operating point. First, a "moving reference" steering angle position was inserted, representing the expected steering wheel position. Second, the muscle forces needed to generate the desired steering wheel angle are calculated by an "inverse internal model", which represents the driver's learnt dynamics of his arms, the vehicle and the steering system. In absence of a capable driving simulator, several test cases were studied to show that the new driver model can describe realistic driver behavior and is capable of realizing large steering angles.

Steering a vehicle during every-day driving situations requires adaptive driver behavior. Optimization is very likely the way drivers constantly (and unconsciously) adapt their parameters such as co-contraction, muscle spindle gain and preview time. Therefore it was shown that the model is capable of describing adaptive behavior by optimizing driver model parameters depending on different driving moods and environment conditions. These optimization routines were subsequently used to obtain different steering system parameter values. Both different environment conditions and driver moods showed to have a substantial influence on the optimal value of the three parameters that were tested. This indicates that there is room for improving steering systems.

2. Introduction

Designing steering systems requires focus on the requirements imposed by the driver. In these are often defined by a "steering feel" which describes the relation between the torque applied to the steering wheel and the resulting steering wheel angle. Segel [39] was one of the first in 1964 to investigate the optimal steering feel. His work is still used by engineers to base their steering system requirements on. Although Segel, among many others (e.g. [28][40]), acknowledged that the desired steering feel is also dependent on the driver, few useful tangible requirements can be found that tie the steering feel to the driver's characteristics or moods. Therefore, traditional design methods rely heavily on evaluation by expert drivers in a time consuming trial-and-error process. Evaluation by test drivers driving prototype vehicles provides the test engineers with only a limited adjustment range. Moving base driving simulators can be used at an earlier design stage since they offer a high steering system modeling flexibility. However, often actuator limits prevent testing of severe cornering situations. Substituting test drivers by a driver model enables the definition of an objective performance metric. Care should be taken to enable modeling of different driving styles, adaptation levels, disturbances and noise sources to realistically model driver behavior. If both the vehicle and the driver are replaced by a computer model, optimization routines can be implemented to quickly find the optimal steering system design.

An important part in vehicle design is the focus on improving safety, which is why nowadays most vehicles are equipped with a so called vehicle stability control (VSC) system. The VSC acts on the brakes, steering wheel, suspension, engine or a combination of these. Typically, the VSC intervenes unexpectedly to the driver, who subsequently cannot use the full potential of the VSC, or even worse: the unexpected VSC actions can trigger a counterproductive panic reaction. Also, VSC activity can lead to a decrease in driver awareness.

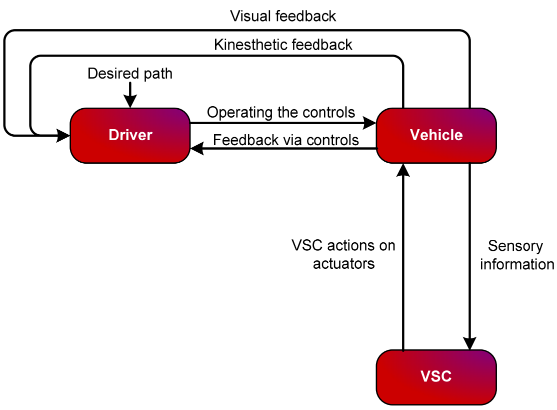

Figure 1. The Driver-Vehicle-VSC control structure where the driver and VSC each receive their own information and operate independently. The driver is not included in the VSC control loop

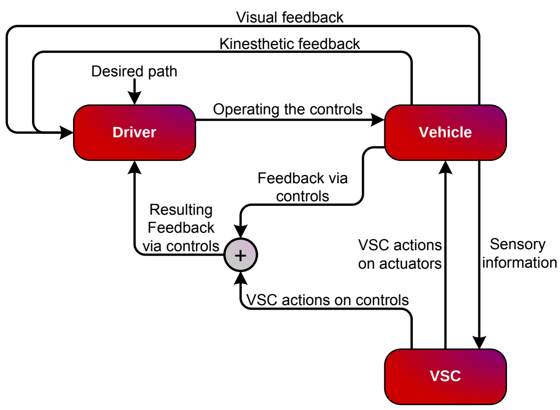

Figure 2. The Driver-Vehicle-VSC control structure where the driver is included in the control loop when the VSC decides to provide the driver artificial feedback via his controls

A VSC system is described in Figure 1; the driver inputs gas, brake and steering actions and receives force and position feedback trough these controls as well as visual feedback from the road and vestibular stimulation caused by the vehicle motion. If the VSC acts on the vehicle, the driver will only notice this indirectly via one of the above mentioned information channels. In Figure 2 a configuration is shown where the VSC directly acts on vehicle actuators as well as on one of the driver controls. This way he is immediately conscious of the VSC information and can decide to cooperate or to resist the VSC feedback. The VSC only bypasses the driver in case the bandwidth of the driver is too low to master the critical situation. Compared to the conventional VSC control system lay-out this can increase driver performance, comfort and awareness.

There are several systems that already apply this principle of including the driver in the VSC control loop. Examples are lane keeping/changing systems [16][17][29], haptic gas pedals [2] and artificial steering wheel torque feedback systems [8]. By providing artificial torque feedback, additional information besides visual can be exchanged. Moreover, the human haptic reflexes holding the steering wheel are much quicker than the visual channel. The reflexes of the shoulder joints have an average bandwidth of 2.5 Hz, depending on the reflexive and intrinsic properties and the configuration of the joints [30], whereas the bandwidth of the visual feedback loop is about 1.0 Hz [31]. Additionally drivers are subject to an extensive amount of visual information, but the haptic senses remain relatively underused. Designing a VSC capable of delivering artificial torque feedback can greatly benefit from the development of a driver model capable of describing the (reflexive) driver response to torque feedback. But also once the VSC is installed in a vehicle, it can benefit from having a driver model in order to constantly tune its actions according to the driver's needs.

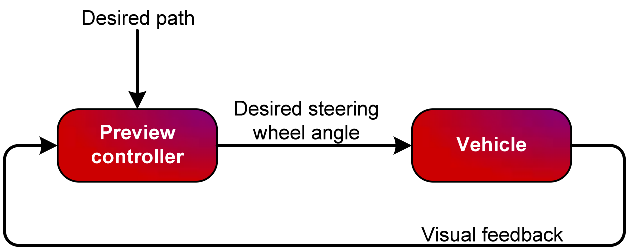

Figure 3. Driver-vehicle control-paths in case the driver is represented by a preview driver model. The driver receives visual feedback only

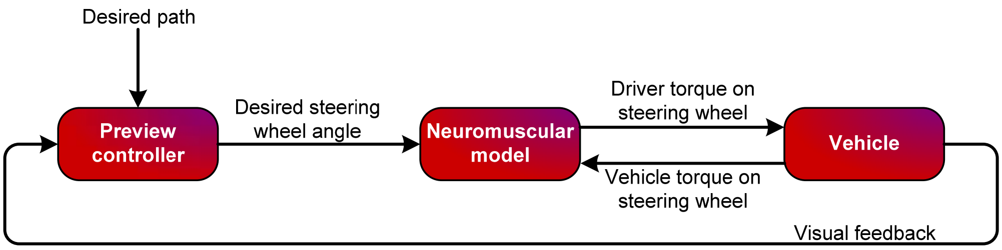

Figure 4. Driver-vehicle control-paths in case the driver is represented by a preview driver model and a neuromuscular model. The driver receives haptic feedback via the steering wheel in addition to the visual feedback

A driver model that has a high potential in fulfilling the above requirements is the neuromuscular (NMS) driver model developed by the Delft BioMechanics group, e.g. refer to [2][9]. This model incorporates limb inertia, instantaneous visco-elasticity from co-contracted muscles, and fast reflexive responses to force and displacement and can be seen as an extension to conventional preview driver models. In Figure 3 such a conventional preview driver model is pictured, controlling the vehicle steering angle using visual information. In Figure 4 a NMS model has been inserted in between the preview controller and the vehicle. In the remainder of this report when referred to a "NMS" driver model, the structure of Figure 4 is depicted. This structure enables a force interface between the driver and vehicle and it is used to develop a haptic gas pedal and a lane keeping system, where it shows promising results [2]. However this model is developed for describing driver behavior only in a single operating point and up to now it has not been used for simulating scenarios where large steering angles are needed, which is a prerequisite for developing a driver model that serves as an objective driver behavior tool for developing steering systems.

2.1. Problem statement

To develop a steering system that enhances driver comfort and safety, the steering system design should be driver oriented. By having a driver model which is able to show adaptive behavior depending on different driving tasks, driver moods and environments, computer optimizations can be employed to obtain an optimal steering feel.

Subsequently the following sub-objectives are derived:

- Check if the current NMS model of the Delft Biomechanics group is suitable for describing scenarios where large steering angles occur.
- Check if all required equations and parameters available.
- Find the necessary neuromuscular aspects which need to be modeled.
- Describe all major benefits of adding a NMS structure to the driver model.
- Enable human adaptation to adapted steering force feedback.
- See if the model can account for different driving styles, if not add to the model.

2.2. Report structure

In chapter 3 a short review on the most frequently used preview driver models is presented, followed by a detailed description of the preview model used in the succeeding chapters. Chapter 4 briefly explains all major parts of the NMS model of Abbink [2] and de Vlugt [9]. To make this model suitable for steering large angles, a new driver model is proposed in chapter 5, followed by a few tests indicating the improvements of the new model in section 5.2. The new NMS model is compared to a single point preview model in section 6.2 in order to show its benefits. In section 6.5 the importance of choosing the right parameter values is indicated, followed by section 6.6 where the adaptive capabilities of the new model asr shown by calculating optimal parameter values that depend on the driving task (lane change or lane keeping) and driver mood (relaxed driving or aiming at optimal path tracking performance). In chapter 7 the benefits are presented of using the newly developed NMS driver model for designing steering systems. Finally, the findings of this report are discussed in chapter 8, the conclusions are listed in chapter 9 and the recommendations can be found in chapter 10.

3. Conventional driver modelling: The preview driver models

Vehicle driver modeling started in the ’50, and initially focused on the compensatory control task of the driver. The driving task at that time was considered to be correcting for external disturbances while maintaining the desired steering wheel position. The scientific field was dominated by researchers from Systems Technology Inc., and mainly McRuer, e.g. [19][20][21][22]. He also developed the widely known and validated crossover model [7], which was one of the first models to describe the human adaptive behavior. McRuer claimed that the driver response is determined by an overall gain, a lead time constant representing the path preview and lag constants accounting for the brain response delay and neuromuscular delay. The second generation of driver models concentrated on the preview path tracking task of the driver, rather than on the compensatory task. The first preview model was proposed by Kondo [26]; it describes how a steering action is decided upon the lateral error between the desired road and the predicted vehicle position a certain distance ahead of the vehicle. Enlightened by his idea, many researchers developed various versions of the preview model. Although they achieved great resemblance with experimental data, the neuromuscular and brain delay (as was the core of the McRuer models) was often not accounted for. The single point preview models were succeeded by models incorporating more than one preview point; but it was not until Macadam wrote his renowned publication [3] in 1980 these were widely adopted. He utilized optimal control theory to calculate the resulting desired steering angle based on the weighted sum of the previewed lateral errors of each preview point. This model is widely used and implemented in several commercial software packages. However since the algorithm of Macadam does not use the yaw angle error as an input, the model is less useful on very curvy roads. Furthermore the Macadam model keeps the input (steering wheel angle) constant during the future vehicle estimation; a problem partly solved later by Ungoren [24]. Still this adjustment is not sufficient for driving trough sharp curves as real drivers tend not to keep the middle of the road as a reference, but they rather follow a “race line”. Also at this point the longitudinal vehicle control of the driver becomes important since it is likely that the driver brakes before or during severe cornering. Moreover because the tires can be well at their limit during severe cornering, the drive/brake torque on the tires can greatly determine the overall vehicle performance. A driver model accounting for most of the above mentioned extensions is the UMTRI model developed in 2000 by MacAdam [23].

Because such a model adds complexity that will eventually blur analysis of the main goal of this report: describing the benefit and use of a NMS driver model, and because of the current disability to validate such a complicated model, a single point preview is used in this report. This model will be used in chapters 6 and 7, and is described in detail below.

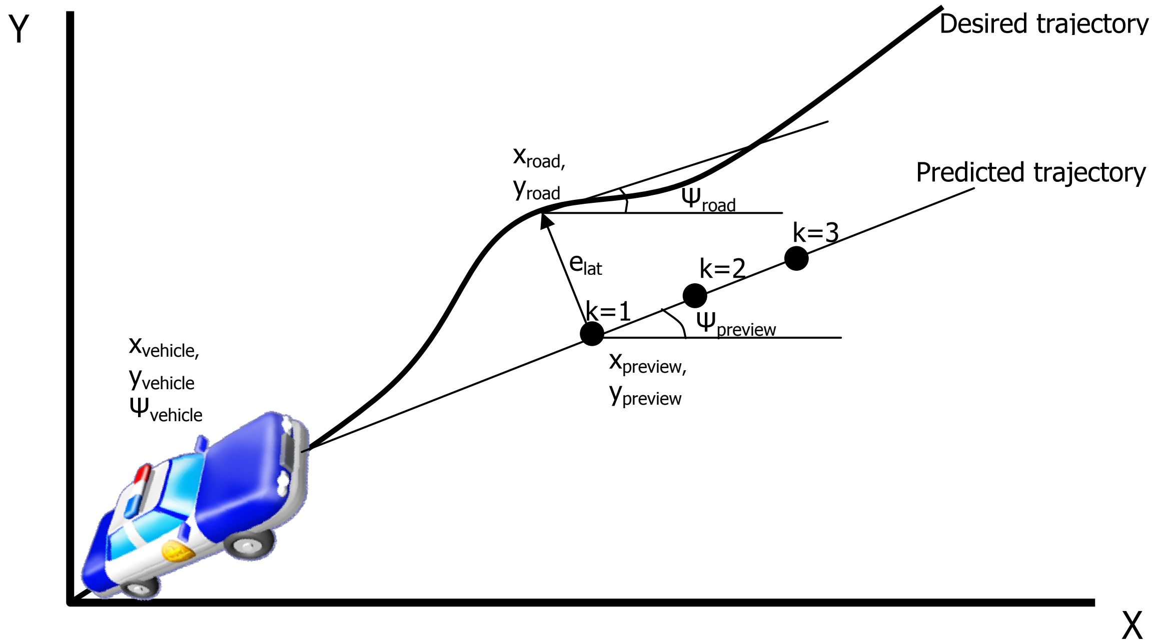

Figure 5. Schematic representation of a preview controller. Here three preview points are pictured (k). The desired steering angle calculated by the preview controller can be tuned by independent gains on the lateral error (e_{lat}) and yaw angle error (ψ_{road} - $\psi_{preview}$) of each preview point.

If in Figure 5 one preview point is used (k=1), the total calculated error is the sum of the lateral error *e* and the yaw angle error. The yaw angle error is defined by the difference between the road yaw angle, Ψ_{road}, and the predicted vehicle yaw angle, $\Psi_{rpreview}$. To calculate the desired steering wheel angle each of the two errors are multiplied by an individual gain and added afterwards. Multi-point preview models often use a weighted sum of the errors of each individual preview point, where points located further ahead are usually assigned a lower weight factor. Additionally, the preview points can be evenly or oddly spaced on the preview distance. A widely used preview model that uses oddly spaced preview points with independent weight factors is developed by Sharp [33]. Instead of estimating the future vehicle position with a simplified model of the vehicle dynamics (as MacAdam and this thesis do, see below), he tunes the preview point gains to match a particular vehicle. The reader who is interested to know more about driver modelling is directed to [34][35][36][37][38], as the next section will continue with describing the single point preview into detail.

The vehicle future position is estimated by using a “bicycle” vehicle model which lumps the dynamics of the two wheels on one axle into one wheel on the x-axis of the vehicle. Equations (1) – (13) describe the dynamical behaviour.

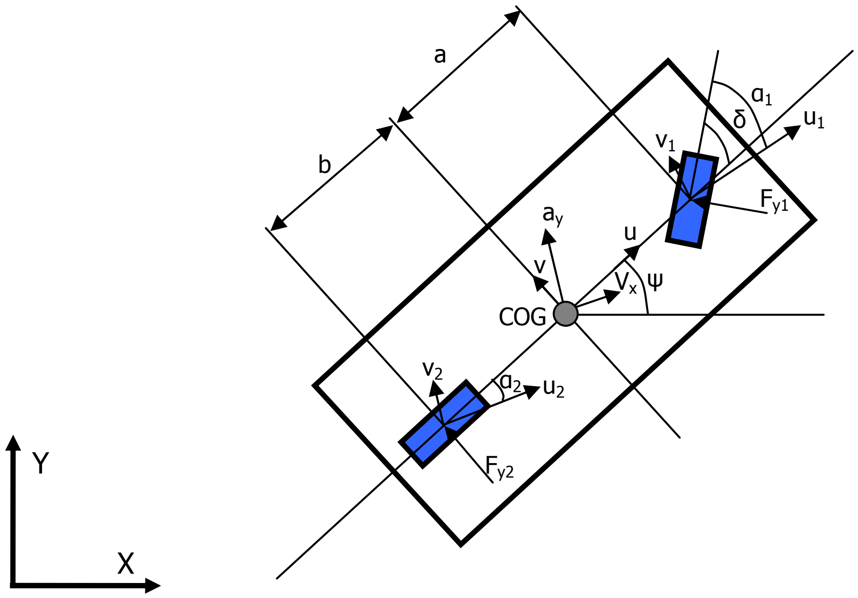

Figure 6. The "bicycle" vehicle model lay-out. This model is used to predict the future vehicle position in the preview controller and it represents the vehicle the driver model is controlling during simulations. Symbols are explained in the text

At first, linear tire characteristics will be assumed, which can be justified only for small slip angles. The resulting lateral forces are presented in eq. (1):

$$F_{y1} = C_1\alpha_1 \text{ and } F_{y2} = C_2\alpha_2 \tag{1}$$

Where C represents the tire cornering stiffness and α the tire slip angle. The subscript 1 refers to the front axle and 2 to the rear axle respectively. The slip angles can be expressed and linearized as:

$$\alpha_1 = \arctan\left(\frac{-v_1\cos\delta + u_1\sin\delta}{u_1\cos\delta + v_1\sin\delta}\right) \approx \arctan\left(\frac{-v_1}{u_1} + \tan\delta\right) \approx \frac{-v_1}{V_x} + \delta \tag{2}$$

$$\alpha_2 = \arctan\left(\frac{-v_2}{u_2}\right) \approx \frac{-v_2}{V_x} \tag{3}$$

With v and u representing the lateral and longitudinal velocities respectively, expressed in vehicle coordinates. The steering angle is noted with δ. Assuming longitudinal speed (u) equals forward speed (V_x). The yaw rate influences the lateral speed per axle:

$$v_1 = v + a\dot{\psi} \tag{4a}$$
$$v_2 = v - b\dot{\psi} \tag{4b}$$

Here, *a* and *b* represent the distance between the center of gravity and respectively the front and rear axle. *Ψ* represents the yaw angle of the vehicle. The substitution of equation (4) in (3), yields equations (5) and (6):

$$\alpha_1 = \frac{-v - a\dot{\psi}}{V_x} + \delta \tag{5}$$

$$\alpha_2 = \frac{-v + b\dot{\psi}}{V_x} \tag{6}$$

The equations of motion read as follows:

$$I\ddot{\psi} = aF_{y1} - bF_{y2} \tag{7a}$$

$$ma_y = F_{y1} + F_{y2} \tag{7b}$$

Where F_y is the lateral tire force and a_y the lateral vehicle acceleration, which can be calculated by:

$$a_y = \dot{v} + V_x\dot{\psi} \tag{8}$$

Substituting in the Newton and Euler equations of motion (7), and moving the state variables to the left hand side results in eq (9) and (10):

$$\ddot{\psi} = -\frac{1}{IV_x}\left(a^2C_1 + b^2C_2\right)\dot{\psi} - \frac{1}{IV_x}\left(aC_1 - bC_2\right)v + aC_1\delta \tag{9}$$

$$\dot{v} = -\frac{1}{mV_x}\left(C_1 + C_2\right)v - \left(V_x + \frac{1}{mV_x}\left(aC_1 - bC_2\right)\right)\dot{\psi} + \frac{C_1}{m}\delta \tag{10}$$

When these equations are substituted in the general state space lay-out:

$$\begin{aligned} \dot{\mathbf{x}} &= \mathbf{Ax} + \mathbf{Bu} \\ \mathbf{y} &= \mathbf{Cx} + \mathbf{Du} \end{aligned} \tag{11}$$

The final state space equation reads:

$$\mathbf{A} = \begin{bmatrix} \frac{-C_1 - C_2}{mV_x} & \frac{-aC_1 + bC_2}{mV_x} - V_x \\ \frac{-aC_1 + bC_2}{IV_x} & \frac{-a^2C_1 - b^2C_2}{IV_x} \end{bmatrix}, \ \mathbf{B} = \begin{bmatrix} \frac{C_1}{m} \\ \frac{aC_1}{I} \end{bmatrix}, \ \mathbf{C} = \begin{bmatrix} 1 & 0 \\ 0 & 1 \end{bmatrix}, \ \mathbf{D} = \begin{bmatrix} 0 \\ 0 \end{bmatrix} \tag{12}$$

With

$$x = \begin{bmatrix} \dot{v} \\ \dot{\psi} \end{bmatrix}, \quad \mathbf{u} = \delta, \quad \mathbf{y} = \begin{bmatrix} \dot{v} \\ \ddot{\psi} \end{bmatrix} \tag{13}$$

The state space system of eq. (12) serves two purposes in this report as it represents the vehicle dynamics used in chapters 5, 6 and 7, and it is used to calculate the future vehicle position. This calculation starts with the initial conditions obtained from the vehicle model: δ, ψ, $\dot{\psi}$, V_x and v. The steering angle, δ, and the vehicle velocity, V_x, are kept constant during the preview calculation, which is executed in n steps. In each step ψ, V_x and v are used to determine the vehicle position, as displayed in eq. (14). The three parameters ψ, V_x and v are found by solving the state space equation of eq. (12) each step. The complete preview calculation process is pictured in Figure 7.

$$X = \int_{T_n}^{T_{n+1}} (\dot{x}\cos\psi - \dot{y}\sin\psi)dt$$
$$Y = \int_{T_n}^{T_{n+1}} (\dot{x}\sin\psi + \dot{y}\cos\psi)dt \qquad (14a,b)$$

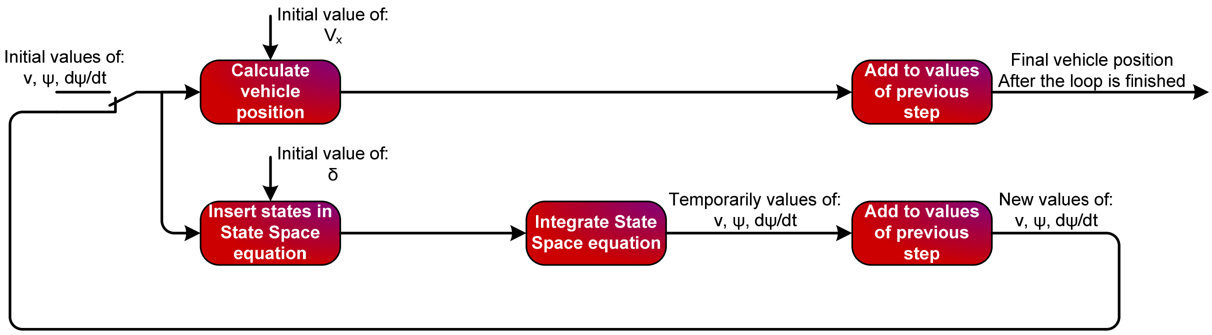

Figure 7. Schematic representation of the future vehicle position calculator. The loop is executed n times and the switch is only set to the upper position for the first step. The initial values are obtained from the state space model that is described in equation (12). The vehicle position is found using equation (14)

In Figure 9 the complete preview model is showed schematically. Equation (14) is used to calculate the global vehicle position in the *global vehicle position calculator,* and the *future vehicle position calculator* represents the structure as pictured in Figure 7. The *local road selector block* reads the actual global vehicle position coordinates (X, Y and Ψ), and passes trough a selection of the total desired road length from the actual vehicle position until a certain position ahead. This point should be located further away than the preview time, but close enough to avoid calculating the error to an incorrect road point. This can occur for example when driving on a circular road. The *error calculator* block calculates the lateral and yaw angle error. The yaw angle error is found by subtracting the (global) yaw coordinate of the predicted vehicle position from the yaw coordinate of the road point closest to the predicted vehicle position. This closest road point, together with the second closest road point is used for calculation of the lateral error, which is obtained by finding the area of the rectangle defined by the sides a, b and c (Figure 8). Side a is located between the nearest road point and the second nearest road point. The resulting lateral error, y, can be found by dividing the area of the rectangle by half the length of a. Finally the yaw error and lateral error each pass trough an individual gain in the *error controller* block and the sum of the two resulting values is the desired steering wheel angle.

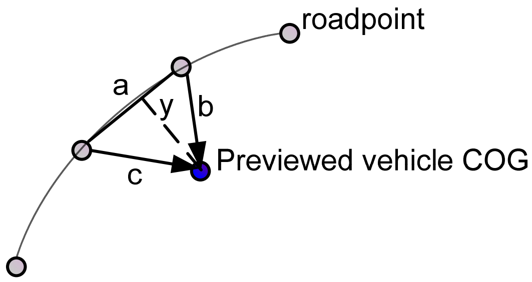

Figure 8. The lateral error calculation between the previewed vehicle position and the desired road. Once the previewed vehicle position is calculated, the nearest and the second nearest road points are determined. The lateral error (y) is found by dividing the area of the rectangle a-b-c by half the length of side a

A brain *processing delay* is added to the model of 0.16 seconds [5]. Rather than being placed in series with the desired steering angle signal, it is placed in series with the desired road generation. This way only a sudden change of desired vehicle trajectory will experience brain processing delay, and not an intended undisturbed trajectory such as a lane change.

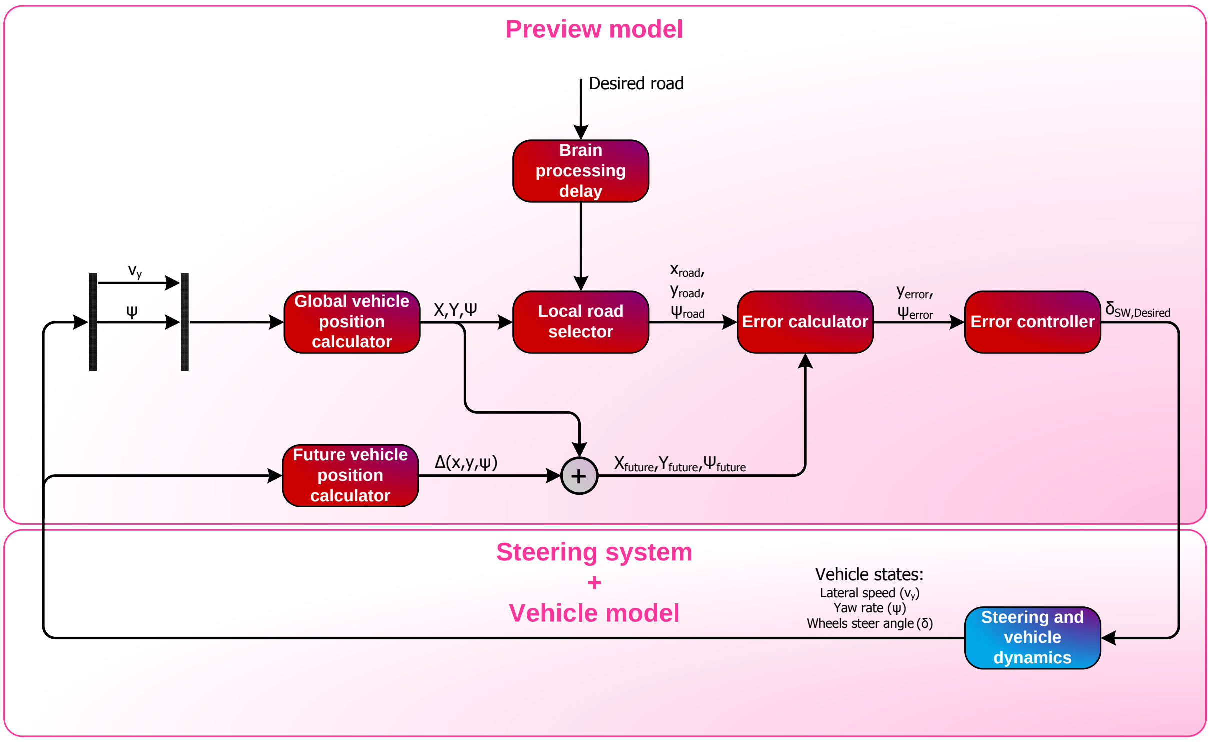

Figure 9. Single point path following controller without NMS structure (based on Kondo [26]) and vehicle model

4. The original neuromuscular driver model

A previewed vehicle position error drives the models in chapter 3 and hence, the error compensation in these models and nearly all its predecessors is limited to a response on visual feedback only (as displayed in Figure 3). It is known that drivers also rely heavily on neuromuscular feedback [4] (as pictured in Figure 4). Therefore kinesthetic features were introduced in a new type of driver models [1][2][5]. They incorporate limb inertia, instantaneous visco-elasticity from co-contracted muscles, and fast reflexive responses to force and displacement. By adding these dynamics the model can describe the driver's physical limits, and reflexes that respond to steering wheel force feed-back.

As mentioned in the introduction, a NMS model can be seen as an additional model that is inserted in between the *error controller* and *steering and vehicle dynamics* block in Figure 9. Pick and Cole [5] developed a comprehensive NMS model structure, as well as the researchers at the Delft Biomechanics group; refer for instance to Abbink [2] and de Vlugt [11]. The latter model contains parameters accurately identified for a steering task [25] with techniques developed by van der Helm [27]. Also, this model includes the hand grip dynamics on the steering wheel and Golgi Tendon Organs, which play an important role during force tasks (see Abbink [2]). Therefore this model is selected as a basis to develop the newly proposed driver model, see Figure 10. Here the complete preview controller of Figure 9 is lumped into the *path following controller* block. In section 4.1 the model structure is explained for each block separately.

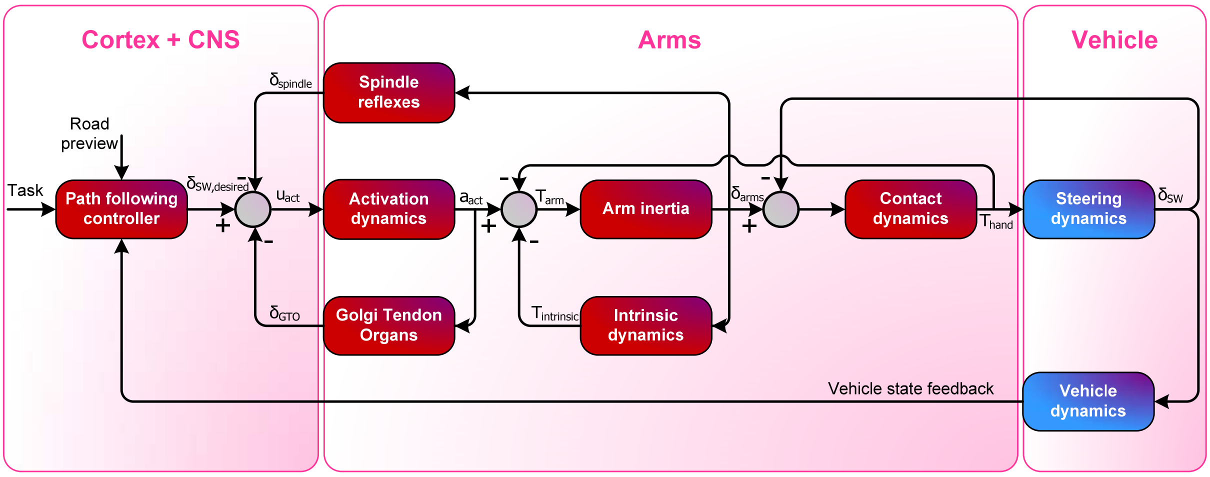

Figure 10. The Abbink [2] driver model building on NMS arm models by de Vlugt [9]. The preview controller and vehicle model which are used in this model are described in chapter 3. The steering system dynamics can be found in section 5.2.1

4.1. Original model structure

The desired steering wheel angle is generated by the path following controller from chapter 3. Since the model is developed to describe the driver's feedback response to small deviations around a steady-state reference steering wheel position, the signal from the path following controller is normally quite low. This signal travels through the nervous system to the muscles, where the *activation dynamics* represent the chemical process converting this nervous signal into muscle forces. The activation dynamics block is modeled as a second order low pass filter, which is described in Chapter 3 of de Vlugt [9], (see eq. (15)). With values of the Eigen frequency $f_{eigen} = \frac{\omega_0}{2\pi}$ = 2.17 Hz and the relative damping, β = 0.74 as found by de Vlugt for the system of shoulder muscles during a posture task.

$$H_{activation}(s) = \frac{1}{\frac{1}{\omega_0^2}s^2 + \frac{2\beta}{\omega}s + 1} \qquad (15)$$

The muscles generate forces that cause the arm inertia to change position. The muscle *spindles* are position and velocity dependent organs which feed back this information to maintain muscle length at a value commanded by the brain. Thus the reflexive muscle activity occurs in response to differences between the actual and expected hand position. The magnitude depends on the gain set by the brain and varies according to the nature of the control task. The system identification methods of Van der Helm [27] were used to unravel the feedback parameter values of the human shoulder muscles. Abbink [25] conducted a position task where the driver had to keep the steering wheel at a fixed position whilst being disturbed by toque perturbations. The identified spindle values of the experiments where the driver was instructed to relax his arms are used, which are 0 Nm/rad for the gain on the position, $K_{p,relax}$ and 0.27 Nm/rad/s for the gain on the velocity respectively. A high muscle spindle gain results in a high bandwidth and better noise rejection without requiring the extra energy needed when using co-contraction. However, since a spinal time delay, τ_{spin}, is incorporated to model the transport time (set to 28.4 ms as identified for a shoulder during a position task [9]), the effectiveness of this feedback is limited at high frequencies. Schouten [10] showed the spindle activity to decrease in case the system has very low damping and/or high frequency disturbances and vice versa. Therefore the central nervous system constantly controls the feedback gains by trading off performance against stability by trying to identify the system the driver is controlling. This will be re-analyzed in chapter 6.

The muscles behave like mechanical spring-dampers of which the damping and stiffness increases with activation level, hence muscles have non-linear mechanical properties. The overall damping and stiffness of a system of muscles contained in the driver's arms is not only determined by the activation levels of each individual muscle, but also by the level of co-contraction. By co-contracting opposing muscles, muscle pairs are stiffened due to the aforementioned non-linear properties of the muscle. As can be seen in Figure 10 the *intrinsic dynamics* account for the increasing damping and stiffness of the driver's arms due to elevated co-contraction. The intrinsic parameters change significantly if the muscles are co-contracted, as was tested by Abbink [25] and Pick and Cole [6][5], who stated that during normal driving elevated co-contraction levels are mainly a sign of drivers inexperience trying to compensate for their own control imperfections or internal noise. However even experienced drivers employ co-contraction in order to be more robust to disturbances and to compensate for their own inaccurate control actions, as will be illustrated in chapter 6. The same identification experiment conducted by Abbink [25] as described also gives us the stiffness ($K_{int,relax}$) and damping ($B_{int,relax}$) values of 4.9 Nm/rad and of 0.69 Nm/rad/s respectively. These properties represent the lumped dynamics of two arms holding a steering wheel. It is likely to assume that, similar to the spindle reflex gain, the co-contraction level is decided upon a tradeoff between the extra stiffness needed to control the system at a certain performance target and the extra energy required to achieve the higher level of co-contraction. Again, in chapter 6 this mechanism will be investigated into more detail.

The *Golgi Tendon organs (GTO)* are sensors which respond to muscle force. They are assumed to have the same neural transport delay as the muscle spindles: 28.4 ms. Spindles and co-contraction are best for position tasks, i.e. when force disturbances should be rejected, whereas force tasks are best accomplished when the subject is compliant and moves along perfectly with the imposed displacements caused by the changing forces. Intrinsic dynamics and muscle spindle feedback are therefore in this case counterproductive. It is hypothesized by [1][9] that during force tasks GTO feedback is pronounced and that muscle spindle feedback and intrinsic dynamics are reduced. How the driver chooses his GTO with respect to his co-contraction level and spindle gains is not clear yet. For reasons of clarity the GTO value is set to zero mainly because we assume conventional steering systems to result in steering being a position task. However if reliable force feed-back systems are developed, the driver can switch from a position tasks to a force tasks by using his GTO feedback, as was found by Abbink [2] who noticed this effect on his development of a haptic gas pedal. The benefit of GTO feedback is the same as using spindle feedback regarding energy consumption: it does not cost extra muscle energy if it is not needed. However, as is also encountered with the spindles, high frequency disturbances can cause instability due to the neural transport delay.

The *contact dynamics* account for the effect that the connection between the hands and steering wheel is not infinitely stiff. Therefore a simple spring and damper characteristic is added between the arm dynamics and the steering system to account for this fact. A stiffness value of 636.86 Nm/rad and damping of 13.27 Nm/rad/s are selected as identified by Abbink [25].

4.1.1. Driver model parameters summarized

All parameters used in section 4.1 are listed in Table 1 to serve as a future reference. Since these values were measured during a relax task, two additional scaling parameters are introduced to model tasks were higher co-contraction levels and/or spindle gains are employed (as in chapter 5 and 6). The first scaling parameter, $u_{cc,}$, represents the co-contraction level, which is 0 if no co-contraction is applied, (and the stiffness, K_{int}, damping, B_{int} are the relax values as shown in Table 1), and is 1 if full co-contraction is applied which is set to 100 Nm/rad for K_{int} and 1 Nm/rad/s for B_{int} [25]. The co-contraction level both scales K_{int} and B_{int} between the relax value and the full co-contraction value. The second scaling parameter adjusts both the spindle velocity gain and position feedback gain. If u_{spin} = 0, the relax values are used as in Table 1 and if u_{spin} = 1, the velocity dependent gain, k_v is 3.37 and the position dependent gain is 8.20, as from [12].

Table 1. Relaxed and tensed driver model parameter values that are used in this report. All parameters originate from literature, except for the correction torque values which are established using heuristic methods

Block	**Parameter**	**Description**	**Value**	**Unit**	**Source**
Torque limiter	T_{limit}	Limit value	50	Nm	[25]
Activation dynamics	f	Bandwidth frequency	2.17	Hz	[11]
	β	Damping constant	0.74	-	[11]
GTO	K_{gto}	Gain	0	-	-
	τ_{GTO}	Delay	28.4	ms	[11]
Arm inertia	J_{arm}	inertia	0.16	kgm^2	[25]
Intrinsic dynamics	$K_{int,relax}$ (u_{cc} = 0)	Stiffness	4.9056	Nm/rad	[25]
	$B_{int,relax}$ (u_{cc} = 0)	Damping	0.6671	Nm/rad/s	[25]
	$K_{int,tensed}$ (u_{cc} = 1)	Stiffness	100	Nm/rad	[25]
	$B_{int,tensed}$ (u_{cc} = 1)	Damping	1	Nm/rad/s	[25]
Spindles	$K_{p,relax}$ (u_{spin} = 0)	Stiffness	0	Nm/rad	[25]
	$K_{v,relax}$ (u_{spin} = 0)	Damping	0.27	Nm/rad/s	[25]
	$K_{p,tensed}$ (u_{spin} = 1)	Stiffness	8.20	Nm/rad	[12]
	$K_{v,tensed}$ (u_{spin} = 1)	Damping	3.37	Nm/rad/s	[12]
	τ_{spin}	Delay	28.4	ms	[11]
Contact dynamics	K_{cont}	Stiffness	636.86	Nm/rad	[25]
	B_{cont}	Damping	13.27	Nm/rad/s	[25]
Correction torque*	P	Gain	0.6	Nm/rad	-
	I	Integrator	4	Nm/(rad s)	-
	D	Differentiator	0	Nm/rad/s	-

* see new model in section 5.1

5. The new neuromuscular driver model

The model of chapter 4 was developed and validated for stationary, near isometric conditions (the condition where the muscle length remains constant) and hence the structure of this model is such that when large steering wheel angles are necessary, as during an evasive maneuver or a rapid highway lane change, significant errors are introduced.
Also the model does not have a structure that converts the desired steering angle to the muscle forces needed to achieve this angle. In the original model of chapter 4 the desired steering angle is directly applied to the input of the model, and therefore the model is unable to take into account the extra muscle force needed due to the dynamics of the system that is controlled.
The new model structure that solves these two problems is presented in section 5.1. Simulations showing that the new model is able to steer during non-isometric conditions can be found in section 5.2.

5.1. New Model structure

5.1.1. A moving reference point

The intrinsic dynamics and muscle spindles of the driver model of chapter 4 can be represented by the system of Figure 11. Here the intrinsic dynamics are modeled by a spring and damper connected to the fixed world to one side and connected to the muscle on the other side. The spindle dynamics feed back the muscle position and velocity with a constant gain to the supra spinal signal originating from the brain.

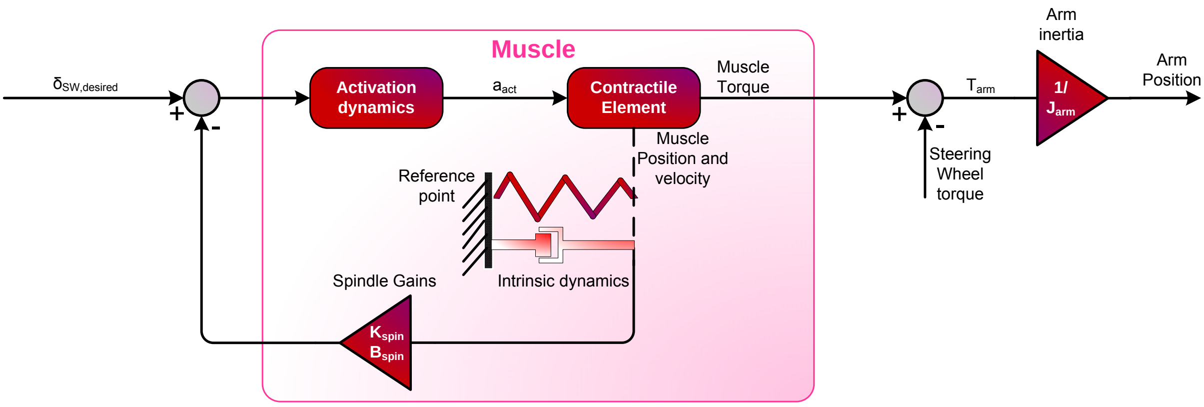

Figure 11. The core of the original driver model of Figure 10 pictured differently to show that the reference point of the intrinsic dynamics and spindle gains is fixed

It can be seen in Figure 11 that for every steering action the driver needs to develop forces to overcome his own intrinsic dynamics and spindle reflexes. This is not realistic. The first step in making the model valid for non-isometric conditions would be to make a moving reference point, which is regarded as the expected muscle position. Only if a steering wheel disturbance causes the expected position to differ from the real position, the reflexes and intrinsic dynamics come into play (called *intrinsic dynamics, CC* in Figure 12). To obtain a more realistic Hill [32] type model structure a Series Elastic element (called *intrinsic dynamics, FF* in Figure 12) could be added in series with the Contractile Element (CE) in

Figure 11 to account for the muscle compliance. Due to the fact that the Parallel Element (PE) has a very minor role during regular movements it is not considered here. Also, non-linear muscle force length and force velocity relationships can be defined, and agonists and antagonists could be separately described. Given the lack of readily available parameters, such a model would not necessarily be more accurate than the current model and no *intrinsic dynamics FF* as displayed in Figure 12 is added to the model at this moment, future work should point out its validity.

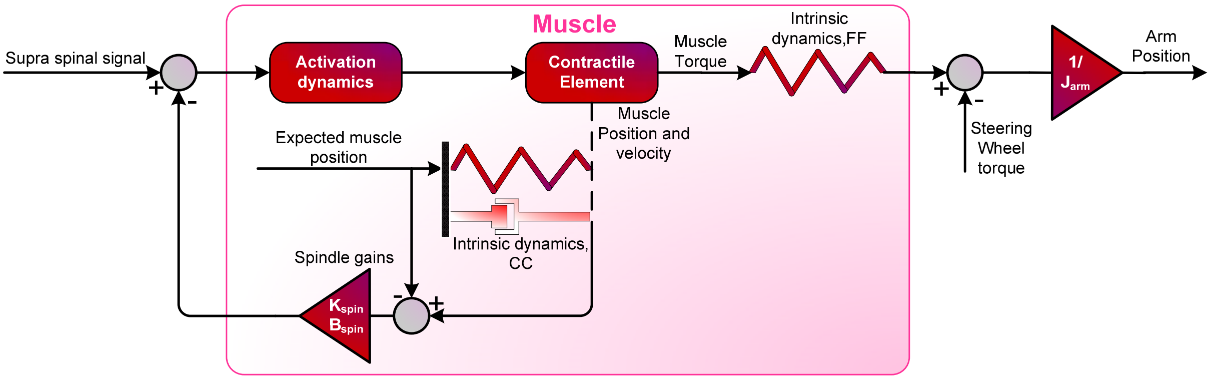

Figure 12. The fixed reference position of Figure 11 converted to a moving reference position to enable realistic transient steering scenarios

The structure as in Figure 12 (but without the *intrinsic dynamics FF*) has been implemented in the original driver model. The moving reference point is the expected muscle position, which could be found by taking the expected steering wheel position if no grip dynamics would be present. Due to the grip dynamics (see chapter 4), the moving reference point is not equal to the desired steering angle. In the next section it is explained how the expected hand position can be found with the aid of the inverse internal model.

5.1.2. The inverse internal model

As stated before, the NMS model of chapter 4 applies the desired steering wheel angle directly to the input of the model. However, the input of the model actually requires a command for the activation level of the muscles. The desired steering angle can only be reached if the exact required muscle force is commanded. One way to achieve this is by inverting a model of the dynamics of the NMS and the vehicle. The resulting inverted model subsequently has a desired steering angle as input and a muscular control signal as an output. The inverse model implemented in the new NMS model is actually split in two parts (the NMS and the vehicle inverse model) which are connected in series (see Figure 13). This enables the calculation of the expected hand position which is needed as a moving reference point for the reflexes. A fifth order 100 Hz Butterworth filter is integrated in this inverse model in order to maintain a model where the nominator is not of a higher order than the denominator. It is likely that the internal model of the driver has to incorporate some sort of linearized, reduced order version of the complex non-linear vehicle dynamics consisting of dozens of states. The influence of different internal models on the overall driver-vehicle performance will be investigated in chapter 6.

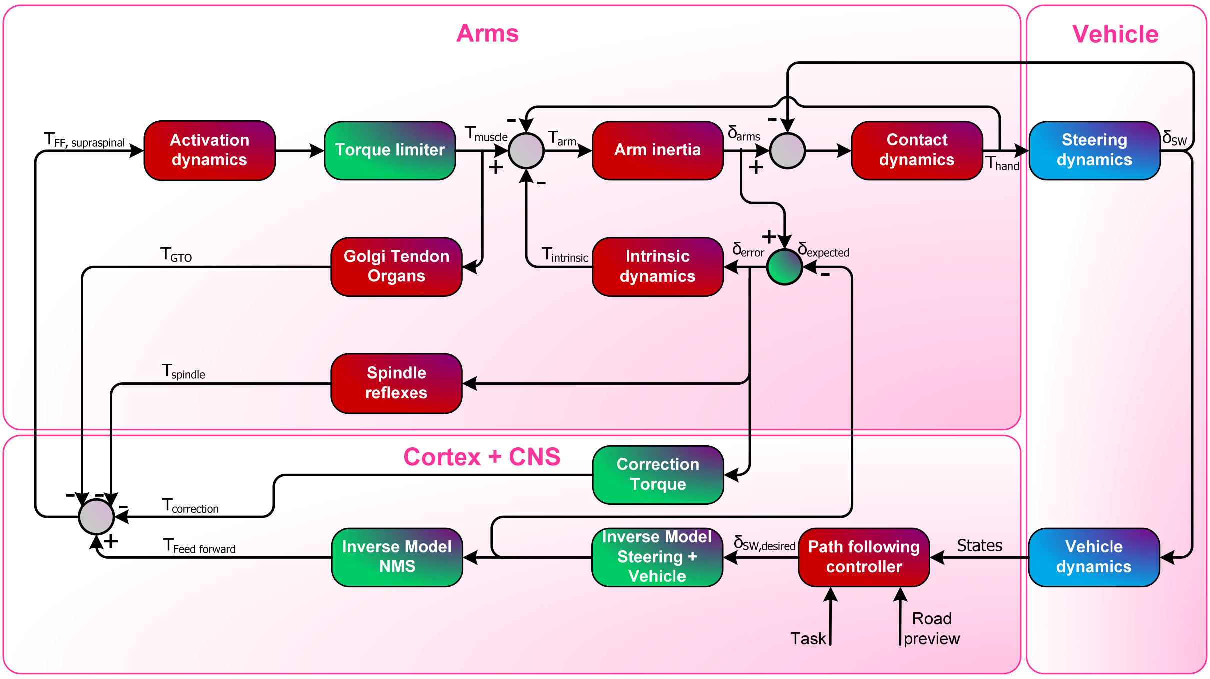

Figure 13. The new driver model structure, based upon the original NMS driver model of Abbink [2] (displayed in Figure 10). While the original NMS model is developed for steering around a fixed steering wheel position, the new model can account for transient steering of large angles. Green colored parts are newly introduced

Because the inverse model has a very high gain at elevated frequencies, the model can output unrealistically high forces. Therefore a *torque limiter* is added in series. This limit is probably related to the length and velocity of the different muscles participating in the steering task and hence a future model expansion incorporating the exact speed-force dependency as determined by Hill [13] is desired. To start with, a fixed maximum value of 50 Nm [25] is implemented. As can be seen in Figure 13 the torque limiter currently limits only the muscle torque as commanded by the brain, whereas part of the available torque is also used for co-contraction. Research is needed as to which extent this limit decreases when elevated co-contraction levels are employed, equation 23 in section 6.5 uses a relation established by Pick and Cole.

The final block to be explained is the *correction torque*. If the inverse model dynamics do not match the real dynamics in a predictable way (for example due to a constant side-wind force disturbance), the driver will most likely not solve this through continuous feedback, but by an adaptation in feed-forward control. Therefore, he should adjust his internal model in order to achieve the desired steering wheel angle. Ideally, the model contains a system identification block to account for the adaptation process of the internal model that occurs in the brain. However in this study a simple PID controller was chosen to compensate for internal model mismatches, which is added in series with a brain processing delay of 0.5 seconds. This delay accounts for the time it takes for the driver to identify the situation and adapt to it. Note that although this block is placed in parallel to the spindle feedback and has a similar function, it has a larger delay and includes an integrating component.

5.2. Driver model comparison tests

In this section the driver models of chapter 4 and 5.1 are connected to a steering system and 2DOF bicycle vehicle model as explained in 5.2.1. Subsequently, a simulation comparing the behaviour of the two models while following a desired steering wheel angle is done in section 5.2.2. Here significant differences are expected since this scenario sparked the development of the new driver model. The simulation comparing the feedback behaviours of the two models to a force disturbance is conducted in section 5.2.3, where the difference is expected to be very low since this is an isometric scenario.

5.2.1. Steering system and vehicle model used for evaluation

Figure 14 visualizes the way the steering system and vehicle model are connected to the new driver model. The 2 DOF vehicle model parameters represent an E60 BMW 530i. The necessary chassis data properties were measured in the Automotive Lab at the Delft University of Technology and taken from the NHTSA [18]. They are summarized in Table 2.
Special care was taken to model the steering system. The driver's hands deliver torque to the steering wheel which is added to the torque in the steering column originating from the tires. The resulting torque accelerates the steering wheel inertia, J_s, which is set to 0.16 kgm^2. A damping constant, b_{sw}, of 0.07 Nm/rad/s counteracts this movement. The rack mass m_r (50 kg) is connected with the steering wheel inertia via the pinion-rack gear ratio i_{swr} (6000 deg/m) and the steering rod with its own stiffness k_s (170 Nm/rad) and damping b_s (0.2 Nm/rad/s). The resulting torque from the difference between the torque applied by the driver, T_d and torque resulting from the tire forces, accelerates the rack mass and its displacement is fed trough a reduction factor representing the suspension kinematics in order to obtain the steer angle of the front wheels corresponding to the steering ratio i_{sw} , which is set to 14.7. No power steering is implemented (T_{assist}) because tis will blur analysis. The front wheel steering angle is used as an input to the state space system as described by equation (12). The outputs of this system, the yaw rate and lateral velocity are used, with the aid of equation (5) to find the front axle slip angle. Multiplying this angle with the tire stiffness, C_f (60 kN/rad) yields the tire side force which is reduced by the tire force to rack force ratio i_{sf} , which is chosen to be 100. This finally yields the feedback of the tire forces on the rack.

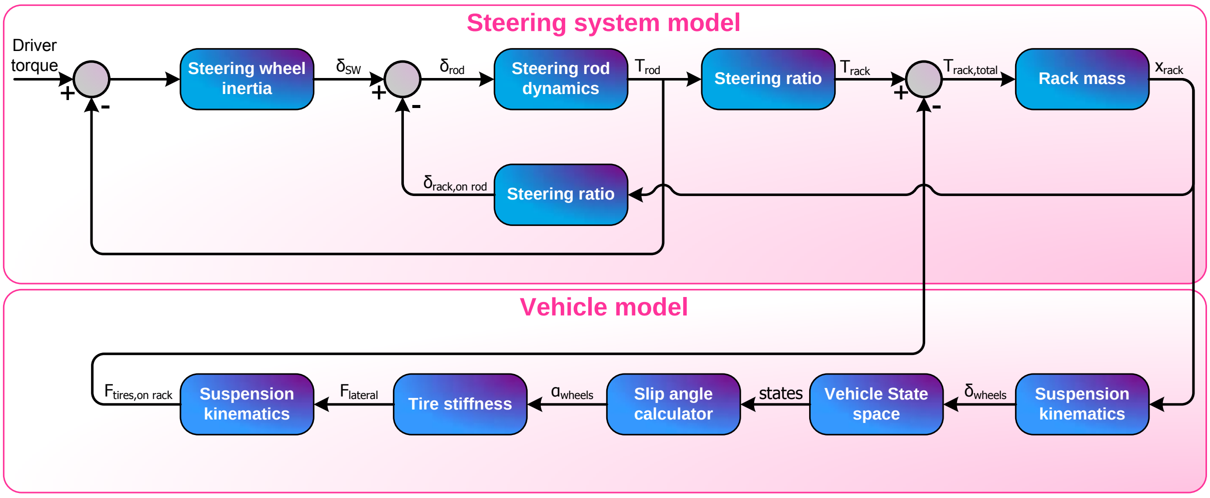

Figure 14. The steering system and 2 DOF vehicle model (see chapter 3), as will be used in simulations to evaluate the driver models

The above described dynamics are depicted in equations (16) to (20). The parameter values used in Figure 15 are explained in Table 2 which are mainly taken from Pfeffer [14].

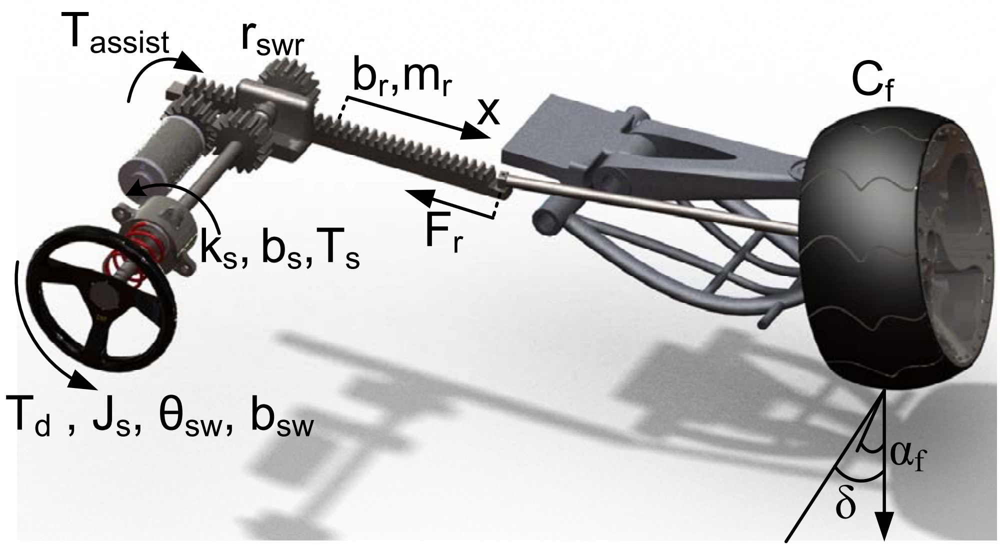

Figure 15. The global steering system lay-out and symbol use. The input to the steering system model is the torque applied by the driver. The output is the steering angle at the wheels, which subsequently passes through the vehicle model of chapter 3 and enables the calculation of the tire side force. This side force passes through a reduction factor, e, to represent the suspension kinematics in order to give the force on the rack, F_r

$$J_s \ddot{\theta}_{sw} = T_d - T_s - b_{sw}\dot{\theta}_{sw} \tag{16}$$

$$T_s = k_s\left(\theta_{sw} - r_{swr}x\right) + b_s\left(\dot{\theta}_{sw} - r_{swr}\dot{x}\right) \tag{17}$$

$$m_r\ddot{x} = \left(T_s + T_{assist}\right) - b_r\dot{x} - F_r \tag{18}$$

With:

$$F_r = \frac{C_f \alpha_f}{e} \tag{19}$$

And

$$\delta = \frac{x r_{swr}}{i_{sw}} \tag{20}$$

Where θ_{sw} = steering wheel angle, T_d = driver torque, x = rack displacement, T_{assist} = power steering assist torque, T_s = torque in the steering rod, F_r = force on the rack originating from the tires, α_f = front wheels slip angle, δ = steering angle front wheels.

To get an impression whether the resulting steering feel is realistic, a Lissajous curve is plotted in Figure 16. Here, a low frequency response of the torque when a sinus shaped displacement profile is imposed on the steering wheel is simulated. In Figure 16 it can be seen that a realistic behavior is obtained. All vehicle and steering system data used are condensed in Table 2.

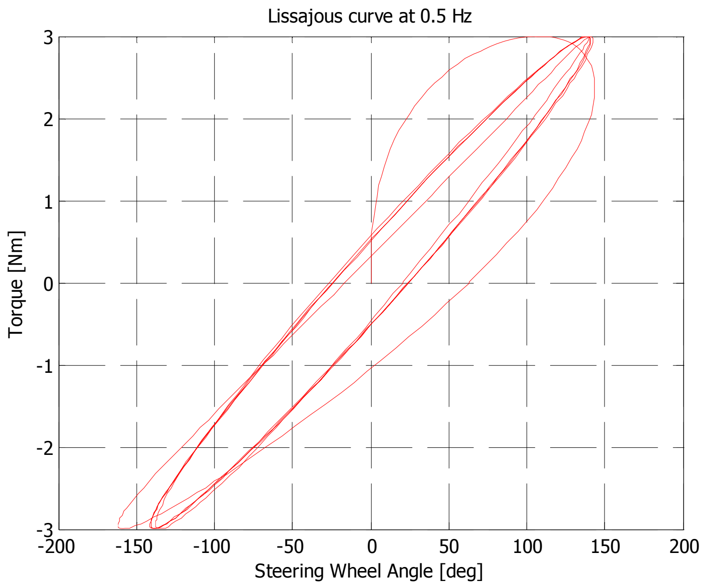

Figure 16. Lissajous curve at 0.5 Hz of the steering wheel angle vs. the steering wheel torque at a reference speed of 80 km/h. This result is used to judge the real life resemblance of the system developed in this chapter

Table 2. Vehicle and steering system parameter values used in this report. The parameters are described per block as displayed in Figure 11. All parameters derive from literature, except for the parameter e (determining the feedback of the lateral tire forces on the rack) and the tire stiffnesses which were linearized from unpublished internal tire data

Block (Figure 14)	Parameter	Description	Value	Unit	Source
Steering wheel inertia	J_s	Inertia	0.16	kgm^2	[25]
	b_{sw}	Damping	0.07	Nm/rad/s	[14]
Steering rod dynamics	k_s	Stiffness	170	Nm/rad	[14]
	b_s	Damping	0.2	Nm/rad/s	[14]
Steering ratio	i_{sw}	Ratio	1:14.7	-	[14]
Rack mass	m_r	mass	50	kg	[14]
	b_r	damping	0	Nm/m/s	-
Suspension kinematics	e	Lumped ratio parameter	100	-	estimated
	r_{swr}	Ratio	6000	deg/m	[14]
Vehicle state space	C_f	Tire stiffness front	60000	N/rad	Linearized from internal source
	C_r	Tire stiffness rear	60000	N/rad	Linearized from internal source
	$J_{z,vehicle}$	Vehicle inertia z-axis	2500	kgm^2	[18]
	$m_{vehicle}$	Mass vehicle	1700	kg	[18]
	a	Distance front axle to CG	1.44	m	[18]
	b	Distance rear axle to CG	1.44	m	[18]
	V	Vehicle speed	(80/3.6)=22.2	m/s	Arbitrarily chosen
Slip angle calculator	V	*-- see above --*			
Tire stiffness	C_f	*-- see above --*			

5.2.2. Feed forward test: steering a desired steering wheel angle

The old and new NMS models are compared in a feed-forward test. Here, feed-forward refers to tests where the model behaviour is dictated by the muscle force commands originating from the brain. Feed-back tests investigate the response to unexpected haptic feedback.

A smooth step input of a desired steering wheel position of 1 rad (see magenta line in centre plot in Figure 17) is applied to the original NMS model (Figure 10) and to the new NMS model (Figure 13). The relax values as displayed in Table 1 are used and the *correction torque* block of the new NMS model is disabled to permit a better comparison. In Figure 17 the time responses at different locations in the model are displayed.

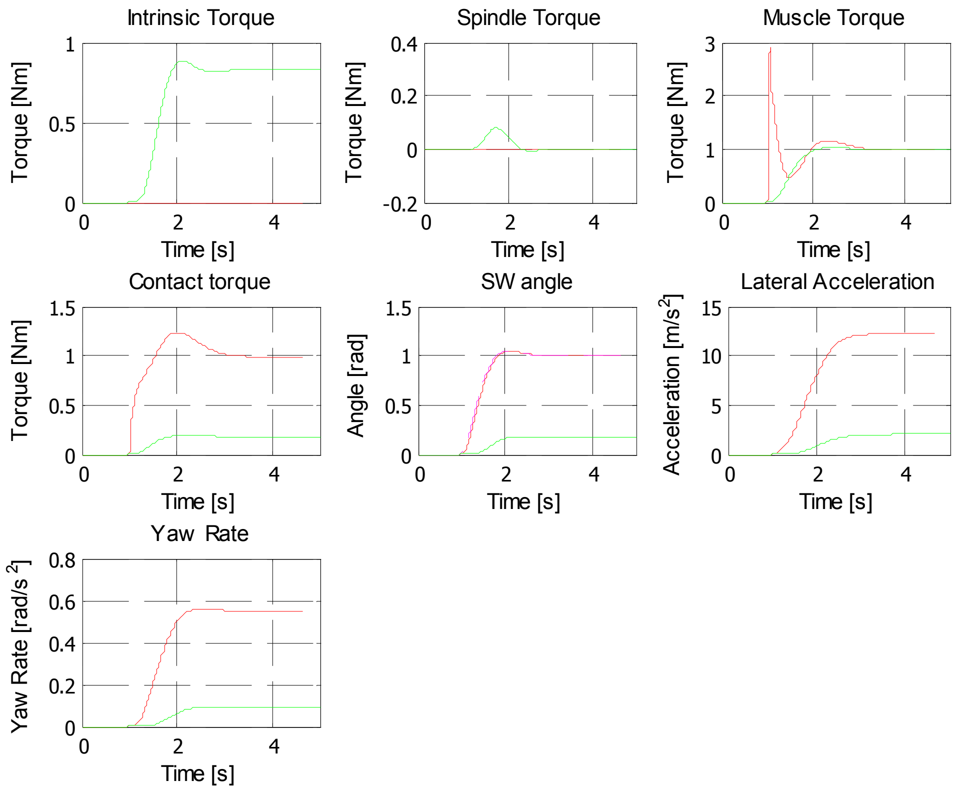

Figure 17. Time responses at different locations within the original NMS model (green) and the new NMS model (red). The input to both systems is a desired steering wheel angle as displayed in the middle plot (magenta). The new model closely follows the desired steering angle whereas the original model is not able to achieve the desired angle

In Figure 17 it can be seen that the new model accurately follows the desired angle. The driver does not show reflexive responses, since he has a perfect internal model calculating the exact forces necessary to obtain the desired steering wheel angle. However the driver as modelled in the original NMS model clearly has to counteract his own reflexes and intrinsic dynamics resulting in the final steering angle being too low.

5.2.3. Feedback test: applying a force perturbation

To investigate the feedback response of the driver models, an unexpected force disturbance is applied to the steering rack. Again, the relax values of Table 1 are used. The disturbance shape has been chosen smoothly to avoid the higher order dynamics associated with a step input (see upper left picture in Figure 18). In Figure 18 the time responses of the original model and the new NMS model can be found, where the latter is represented in four forms:

- Without intrinsic dynamics, reflexes and correction torque,
- Without reflexes and correction torque, with intrinsic dynamics active
- Without correction torque, with intrinsic dynamics and reflexes active
- With correction torque, intrinsic dynamics and reflexes all active.

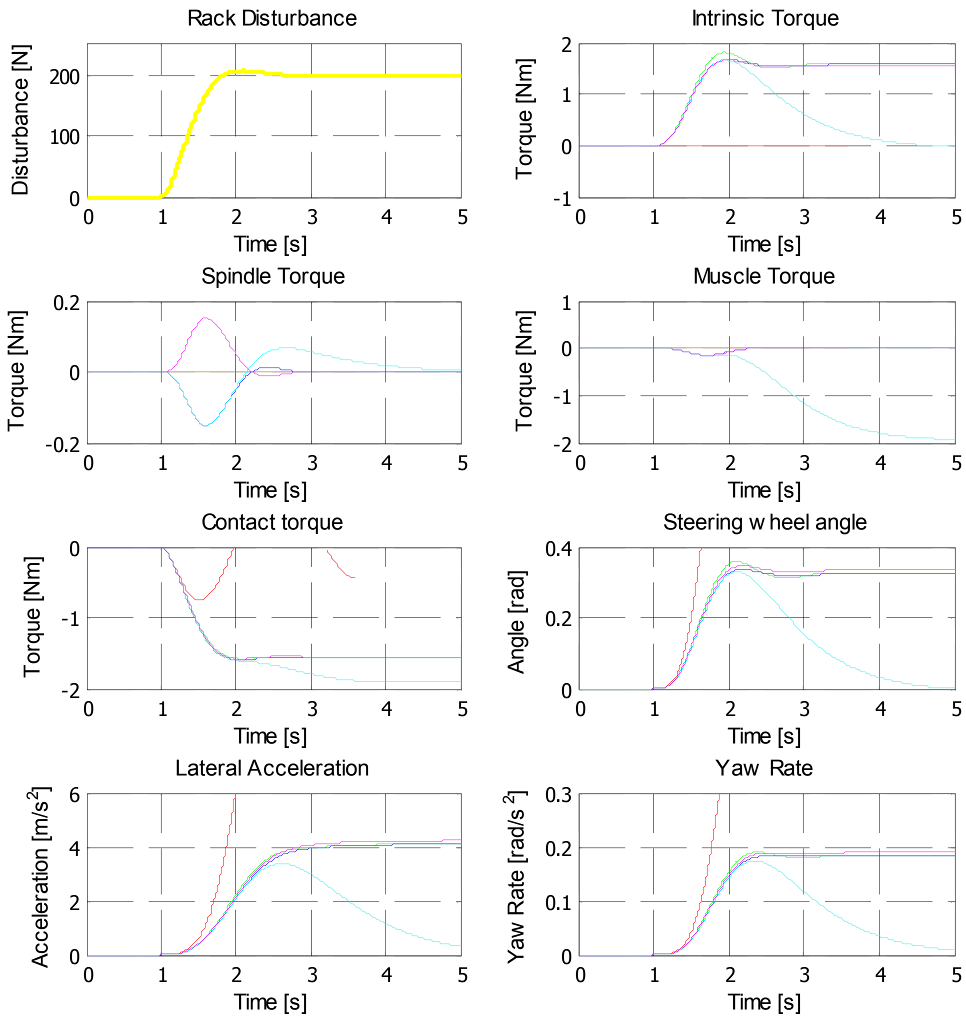

Figure 18. A force disturbance of 200 N is applied to the rack as displayed in the upper left plot. Displayed are: time responses of different parts within the original model (magenta); the new model with no intrinsic dynamics, no reflexes and no correction torque (red); the new model with the intrinsic dynamics active, no reflexes and no correction torque (green); the new model with intrinsic dynamics and reflexes active and no correction torque (blue); and the new model with intrinsic dynamics, reflexes and correction torque all active (cyan)

In Figure 18 it is evident that the best disturbance rejection is delivered by the model with the correction torque loop. It is able to completely compensate for the disturbance within 4 seconds. The red line represents a driver with only the inertia of the arms and no stiffness or damping applied, which eventually gets unstable. The original model shows in this case the same result as the new model, since the desired steering angle is zero degrees (so no inverse internal model affects the response) and the reference position for the reflexes is also at zero degrees for both models. Finally it should be noted that the current co-contraction and intrinsic reflex gains are very low and increasing them could greatly improve performance in this case.

6. The key to building a realistic model: Parameter analysis

The newly proposed NMS driver model can describe more realistic behavior compared to the original NMS model. A moving reference point enables transient steering and the internal model ensures that the (by the driver estimated) correct muscle forces are commanded in order to achieve the desired steering wheel angle. The driver model parameters as showed in Table 1 are validated for a constant steering wheel angle (zero degrees in this case) and for a constant task (position a dot on the screen inside a box, without co-contraction). Steering a vehicle during every-day driving situations will require changing steering wheel angles, vehicle positions and co-contraction level. Optimization is very likely the way drivers (unconsciously) choose their parameters such as co-contraction, muscle spindle gain and preview time, therefore in this chapter the new model itself is used to determine the parameters by assuming that the driver selects them by using optimization techniques. This will show the adaptive capabilities of the driver model.

It is hypothesized that the driver adapts his parameters according to two main conditions: the mood of the driver and the task he has to perform. Different driver "moods" are defined in section 6.5. Subsequently, in section 6.6 the driver model parameters are optimized. The degree to which the internal model of real drivers matches the real NMS and vehicle dynamics is still to be determined. However, to get a feel of the sensitivity of the internal model, the effect on driver performance of equipping the vehicle with non-linear tires is examined in section 6.3. Also, less competent drivers are simulated in section 6.4 where the order of the inverse internal model is lowered. But before this, in section 6.2 the new model will shown to be superior to a preview driver model. The values of the preview parameters are determined in section 6.1 together with the introduction of a double lane change test road.

6.1. Adding a preview structure to the NMS model

The single point preview model described in chapter 3 is added to the new NMS model. In the following sections this resulting model will be used to perform double lane change maneuvers and perturbed lane keeping tasks. The center line of an ISO 3888-1 double lane change is chosen as a reference road, with the vehicle forward velocity set to 80 km/h. The desired road trajectory is visualized in Figure 19.

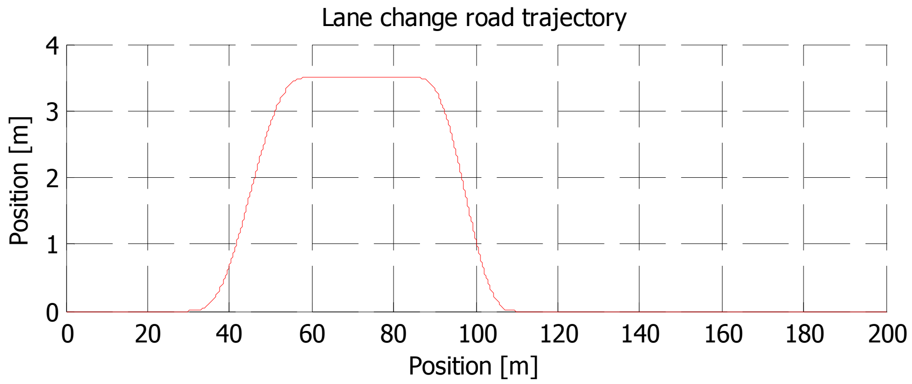

Figure 19. The trajectory of the middle of the road of an ISO 3888-1 double lane change, test velocity is 80 km/h

The preview model contains three parameters of which the value has to be established; the look-ahead time, the gain on the previewed lateral error and the gain on the previewed yaw angle error. Realistic vehicle behavior is maintained by taking care not to exceed 1.0 g lateral acceleration during the lane change. If the preview control gains are high, the linear tire model easily allows for lateral acceleration values up to 2.5g due to the non-saturating tire stiffness. In Figure 20 the lateral accelerations and the vehicle trajectories are plotted for gain values aiming at absolute maximum performance and aiming at maximum performance with a limit of 1 g lateral acceleration respectively.

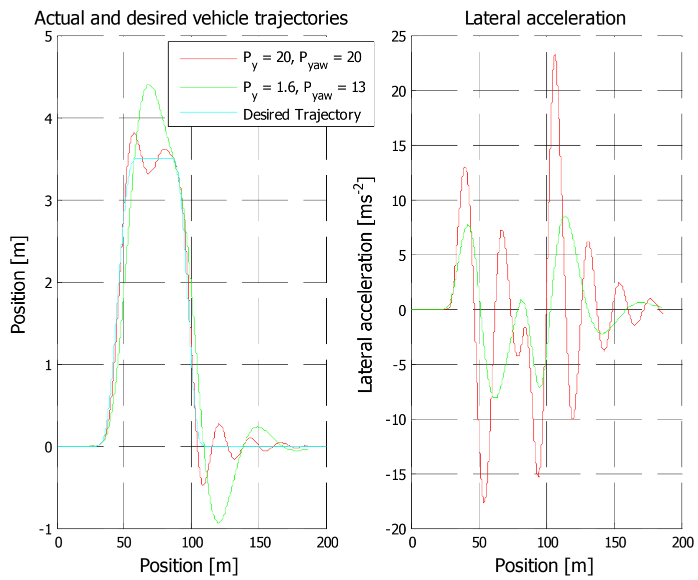

Figure 20. Vehicle trajectories and lateral accelerations for two sets of preview controller gains; red = P_y = 20, P_{yaw} = 20; green = P_y = 1.6, P_{yaw} = 13. Whereas the red line can follow the desired trajectory with a higher accuracy, the lateral accelerations are unrealistic. The green line displays acceptable path tracking performance while maintaining realistic lateral acceleration values

As can be seen in Figure 20, having a lateral error gain $P_y = 20$, and a yaw angle error gain of $P_\psi = 20$ results in the best path tracking performance. However 2.5g lateral acceleration is not a realistic value. Furthermore, as will turn out in Figure 33 and Figure 34 these values are very good in achieving the best performance, but at the cost of mental and physical workload. Although having more realistic lateral acceleration values, the performance of the green line (P_y = 1.6, P_ψ = 13) in Figure 20 is moderate, especially during the first curve the controller seems to act too late. This is because the preview time is set to only 0.2 seconds. Increasing the preview time will improve performance in the first curve, but will also cause instability in the following curves due to the increasing previewed errors. More sophisticated preview models are required for simulating the path tracking behavior more realistically during this extreme maneuver.

6.2. Comparing a preview and NMS model

In this section a preview driver model as described in chapter 3 is compared to the new NMS model. The driver models again are coupled to the vehicle and steering system of section 5.2.1 (Figure 14), together with a desired road profile and preview parameter values determined in section 6.1. When conducting the lane change, the preview driver model and the NMS driver model with or without co-contraction all show the same behavior in Figure 21. This is because if the NMS driver model contains a perfect internal model of his own arm dynamics and the dynamics of the vehicle, it knows exactly which muscle forces to command in order to steer the trajectory as desired by the path following controller in the brain. Only in case the desired muscle forces are too high, the vehicle trajectories will differ due to the physical limitations that are embedded into the model.

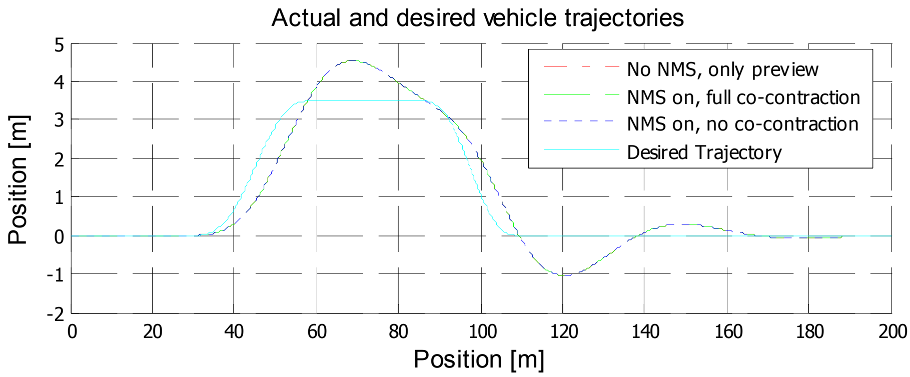

Figure 21. Vehicle trajectories during an undisturbed lane change task; the red line represents a preview model without NMS structure (hence only visual feedback); the green line shows the response of the new NMS model with full co-contraction (u_{cc} = 1); the blue line represents the new NMS model with no co-contraction (u_{cc} = 0); the desired trajectory is pictured in cyan (results of the three models are virtually identical). The moderate path tracking performance is a result of the high vehicle velocity (80 km/h) and the limits of the single point preview controller

If a perfect inverse model is used, and no force disturbances are introduced into the vehicle-driver system, there is no benefit of adding a NMS structure to a preview driver model. However if the realized steering wheel position does not match the desired position due to either wrong feed forward control actions of the driver (wrong path planned, wrong error control method, or wrong muscle force commands) or due to force disturbances transmitted from the tires to the steering wheel, the behavior of a conventional preview driver model will differ compared to the newly proposed NMS driver model.

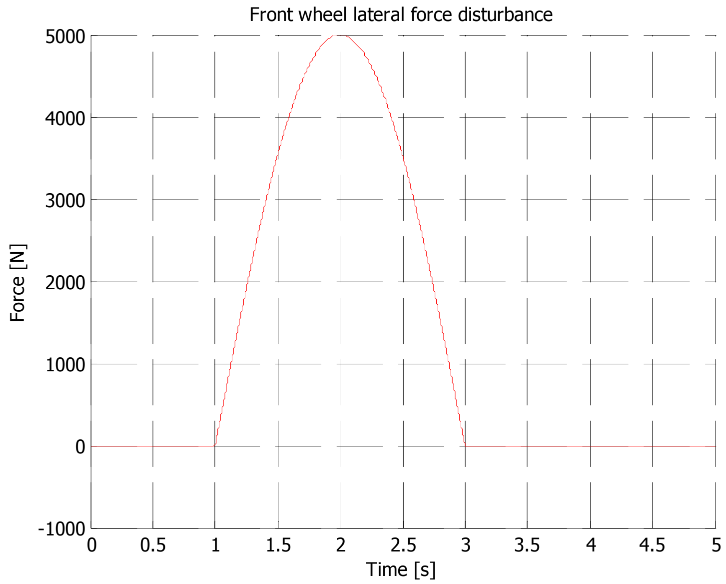

Figure 22. Force disturbance as applied to the front wheels

The next test is a lane keeping task where an unexpected lateral force disturbance of 5000N is applied to the front axle as seen in Figure 22. The preview values are obtained from section 6.1 and the NMS values are listed in Table 1. The resulting vehicle behavior when controlled by three different model settings (only preview, NMS with no co-contraction and NMS with full co-contraction) can be seen in Figure 23, where the benefit of adding a NMS structure is clear. By using full co-contraction the disturbance can almost be completely compensated. The delay of the vehicle dynamics and the brain processing, which is set to 0.16 seconds (and can be many times higher in real life), allows the vehicle to travel significantly more in lateral direction compared to the NMS model. Hence using a driver model without a NMS system or having a vehicle which prevents the NMS dynamics of the driver to act due to no feedback will result in a significantly less controllable vehicle.

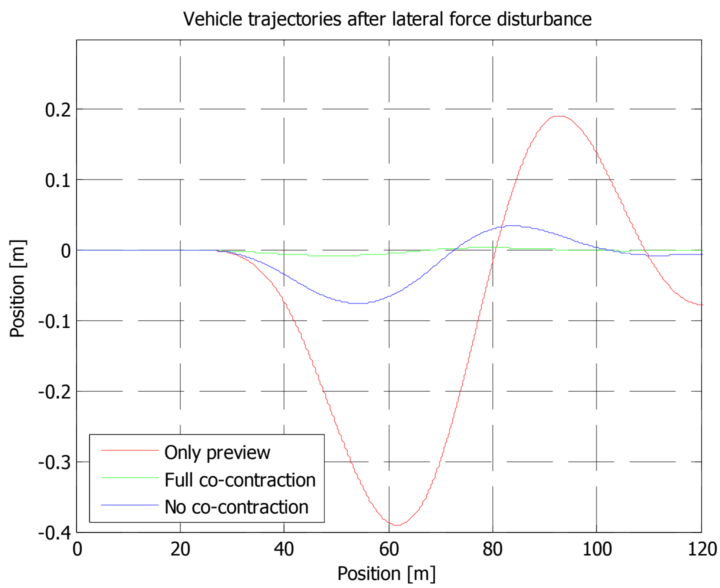

Figure 23. The result of an unexpected force perturbation on vehicle trajectories during lane keeping (see Figure 22 for disturbance characteristics). Three responses are shown: only visual response to the resulting lane-keeping error (red line), the combined visual and neuromuscular response in case the driver is relaxed (blue line) and in case the driver is actively resisting force perturbations (green line). Corresponding parameters for relaxed state and resisting state are shown in Table 1.

6.3. Linear vs. non-linear tires

The linear tire stiffness of the vehicle model is replaced by a non-linear "magic formula" tire model developed by Pacejka [15], see equation (21).

$$F_y = D\sin(C\arctan(B\alpha - E(B\alpha - \arctan(B\alpha)))) \tag{21}$$

Where α is the tire slip angle, and the values of B, C, D and E can be found in Table 3. The normal force, F_z, is obtained from Table 2.

Table 3. Pacejka's "magic formula" tire parameters

Parameter	**Value**
B	9.0
C	2.4
D	$= F_z = 8500$
E	1.0

The linear and non-linear tire characteristics are pictured in Figure 24. During the lane change simulations where the vehicle is equipped with the non-linear tires, the inverse internal model still bases his actions on the assumption that the vehicle is equipped with linear tires. To increase the effect of changing to non-linear tires, the initial non-linear tire stiffness is higher than the linear variant, only to decrease rapidly after about 4^0 slip angle. The resulting effect is displayed in Figure 25, where the lane change of Figure 19 is conducted again.

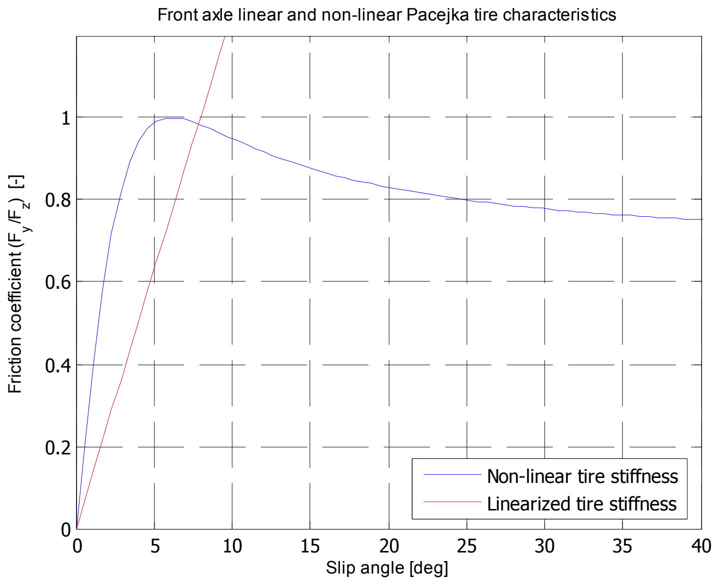

Figure 24. The tire characteristics of the linear tire stiffness as modelled in chapter 3 (red line), and a Pacejka [15] non-linear tire stiffness of equation (21) (blue line). The rear axle has the same characteristics as the here pictured front axle

The first thing that is noticed when viewing Figure 25 is the fact that the non-linear tires show better path tracking performance than the linear tires. This is due to the fact that the tire stiffness of the non-linear tires is higher at small slip angles (see Figure 24) compared to the linear tires which makes up for the late reaction of the preview model in the first corner. Secondly, the high lateral error preview gain which tries to make up for the lateral error caused by the short preview time causes quite some steering angle overshoot in the second corner. Non–linear tire characteristics damp out this effect, since they limit the side force at large steering angles.

Coming back to the comparison between the preview and NMS model, only very minor differences are noticed. Changing the tire stiffness ratio between front and rear appears to have a more profound effect as showed next, where again linear tire stiffnesses are used.

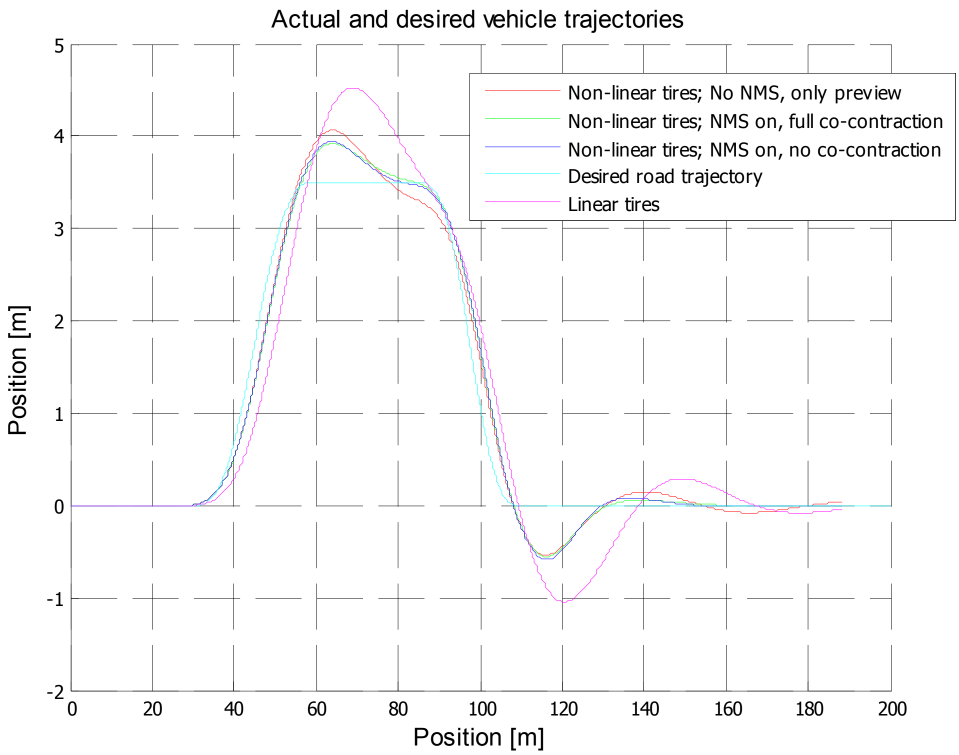

Figure 25. Vehicle trajectories during a lane change task. The magenta line is the reference condition (same as Figure 21), all other 3 simulations were done with the vehicle equipped with non-linear tires (Figure 24) while the internal model based its actions still on linear tire characteristics. The red line represents the resulting driver behavior without NMS (visual feedback only), the green and blue lines represent the driver behavior with full co-contraction and relaxed state respectively. Values used are found in Table 1 (all values in relax state)

In Figure 26 the result of another lane change simulation is displayed. Here the internal model remains constant (with the assumption that the vehicle is equipped with equal front and rear tire stiffness). The tire stiffnesses are linear. The red line represents the case when the tire stiffness ratio between front and rear is exactly as estimated by the driver, the green line represents an oversteering vehicle, the magenta line represents a heavily oversteering vehicle, the blue line pictures an understeering vehicle and the cyan line is the desired road. Understeering vehicles show a bad path tracking performance since the driver increases his steering angle to compensate for the increasing error. The best thing to do in this case would be to countersteer and regain a higher stiffness. Oversteering vehicle configurations track the path quite well until the oversteering is too severe and the vehicle becomes uncontrollable.

It is interesting to note that only after reducing the rear tire stiffness to one sixth of the front tires stiffness, the vehicle becomes noticeably harder to control. As we saw in the preceeding section, equipping the vehicle with non-linear tires also did not have a big impact on the vehicle stability.

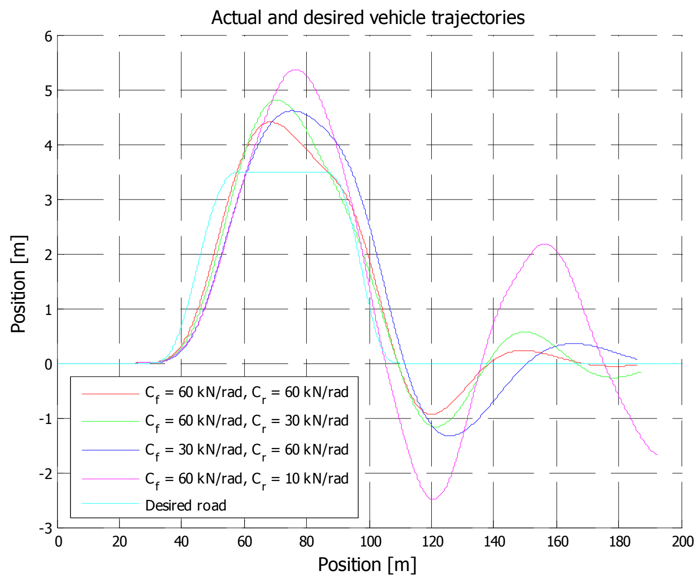

Figure 26. Vehicle trajectories during a lane change. The red line is the reference condition (same as Figure 21), in all other 3 scenarios the (linear) front or rear tire stiffness was changed while the internal model was not corrected for the change. The green line shows the vehicle trajectory when the rear tire stiffness is half the original stiffness, the blue line represents the path tracking after decreasing the front tire stiffness with 50% and the magenta line shows the vehicle trajectory in case the rear stiffness is only a 6th of the front tire stiffness at the rear. The cyan line pictures the desired road

6.4. High vs. low order internal model

Until now the driver is assumed to have a perfect inverted, linearized version of the NMS and vehicle dynamics. This internal model is of 11th order. In this section we will explore the impact of having three different internal models which are less accurate than the 11th order model. The first two internal models to be tested are a mass-spring-damper (2nd order) and a spring (zero order) representation of the original 11th order model. Also, the effect of neglecting the NMS dynamics (see the inverse NMS dynamics block in Figure 14) is tested by implementing an inverse model of only the vehicle. The bode plots of these four models can be seen in Figure 27.

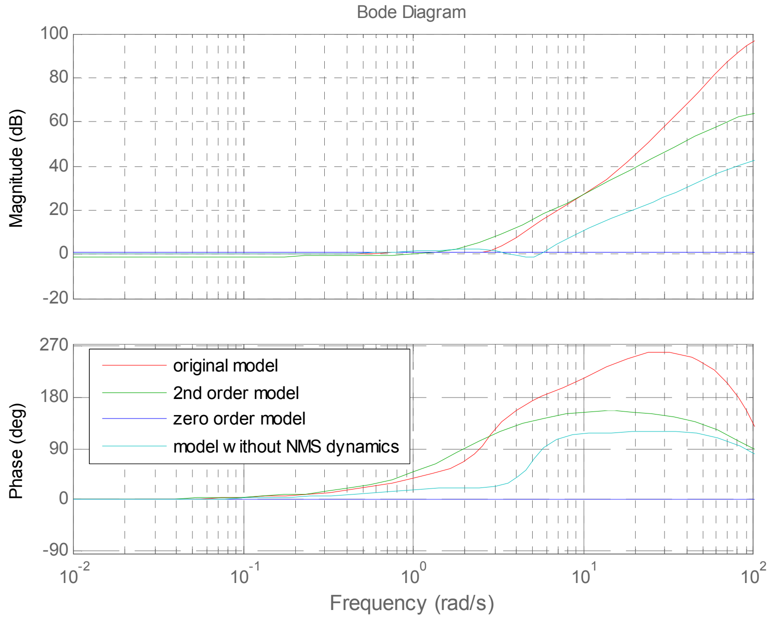

Figure 27. Bode diagram of different internal models. The red line represents the reference internal model dynamics, where the internal model is equal to the inverse dynamics of the NMS and vehicle dynamics. The green line is a 2^{nd} order representation of the reference 11^{th} order model, the blue line represents the dynamics after the original model is reduced in order to a zero order model, and the cyan line pictures the dynamics of the internal model where the driver has only gained knowledge of the vehicle dynamics and neglects his own NMS dynamics. The input of all internal models is the desired steering wheel angle and the output is calculated muscle torque

For each of the four different internal models (shown in Figure 27) the ISO double lane change is simulated. The simulation results are shown in Figure 28.

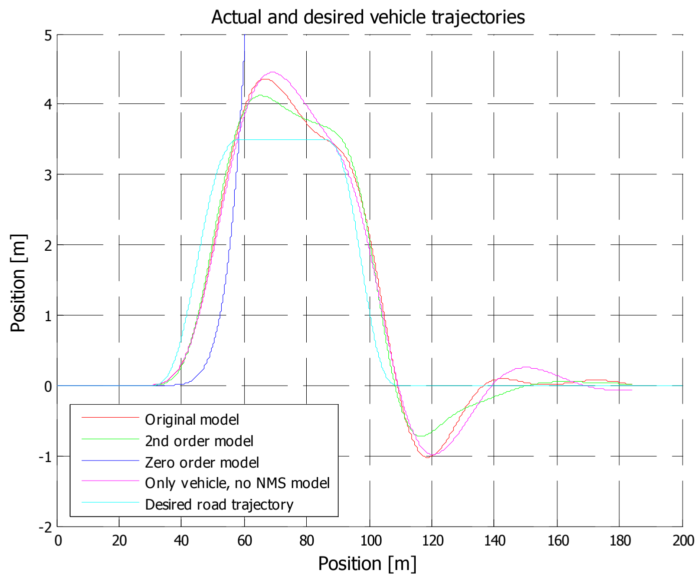

Figure 28. Vehicle trajectories during a lane change with the different internal models as pictured in Figure 27. The red line represents the original 11^{th} order model, the green line the 2^{nd} order approximation, the blue line the zero order approximation, and the magenta line the original model without inverse NMS dynamics. The cyan line is the desired trajectory

Interestingly, the second order approximation outperforms the original model, because it has a lower gain at the high frequency output of the preview controller in the second corner which compensates for the high preview gain on the lateral error. The zero order representation cannot follow the desired road because it lacks the increase in gain at high frequencies. The driver with an internal model assuming there are no dynamics in his NMS system seems to cope quite well with this handicap. This is mainly thanks to the big difference between the real steering angle and the desired angle. Therefore, the intrinsic dynamics and spindle reflexes help delivering the extra torque required to complete the lane change successfully. In Figure 29 it is clear that the intrinsic torque delivers up to 3 Nm, whereas all other three cases hardly use their intrinsic dynamics. For comparison: 3 Nm of muscle torque can steer the steering wheel 150 degrees, see Figure 16. The second order model needs only 0.01 Nm or intrinsic torque and the 11th order model none at all (zero order not regarded here due to its inability to complete the lane change).

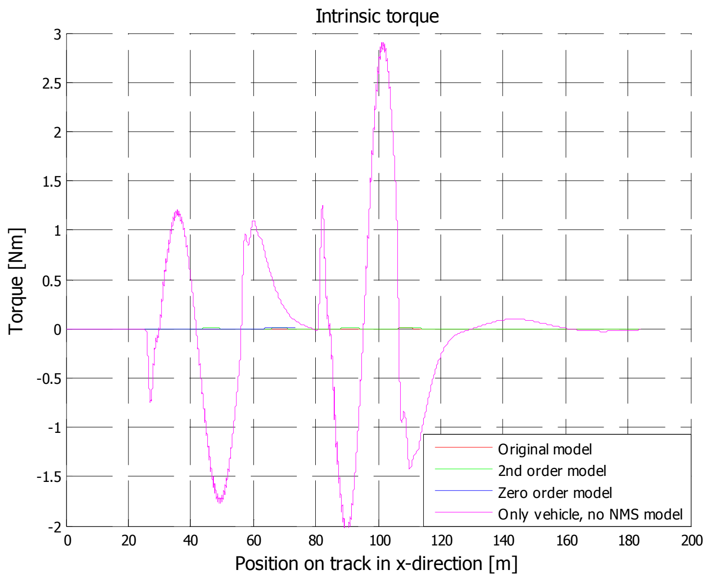

Figure 29. Intrinsic torque for the simulations as pictured in Figure 28. In Figure 28 it can be seen that the driver neglecting his own NMS dynamics still shows reasonable performance. In this figure it is clear that the intrinsic torque is responsible for this, using up to 3 Nm to maintain the desired steering wheel angle. 3 Nm of muscle torque is enough to steer the steering wheel 150 degrees when the vehicle travels at 80 km/h (see Figure 16). All other lines (red, green and blue) are within the 0 – 0.01 Nm range

6.5. Parameter variation

Already in 1964 Segel [39] suggested that the degree to which the steering wheel affects driving is dependent upon the type of control strategy used to drive: either “free control” driving which is relaxed or “fixed control” driving which is a high gain task. In this section five driver model parameters are selected and changed while monitoring the effect on three cost criteria representing different types of “control strategy”, or “moods”. They are the path tracking accuracy of the vehicle (P), the mental workload (MW) and the physical workload (PW). A low PW has the obvious benefit of requiring low energy levels, and therefore the driver is able to fulfill his task for a longer period. A low MW will allow the driver to quickly react in dangerous situations. This way the sensitivity of the model to each parameter can be checked. At the same time it can be seen if the formulae used to calculate MW and PW are reasonable.

The first parameter to be sensitivity analyzed is the co-contraction level, u_{cc}. As displayed in Table 1, full co-contraction and no co-contraction is represented by u_{cc} = 1 and u_{cc} = 0 respectively. The second parameter is the muscle spindle position and velocity feedback gain, u_{spin}, which works analogous to u_{cc} and is also listed in Table 1. The following three parameters originate from the visual controller: the preview time, T_{prev}, the gain on the previewed lateral error, P_y and the gain on the previewed yaw angle error, P_ψ. All parameters under sensitivity analysis are summarized in Table 4.

Table 4. Parameters of which the optimal value will be obtained via optimizations to different driver moods, for different driving tasks

Parameter to be changed	Description
u_{cc}	Co contraction level
u_{spin}	Muscle spindle position and velocity feedback scaling gain
T_{prev}	Look ahead time preview controller
P_y	Gain on the lateral error, preview controller
P_ψ	Gain on the yaw angle, preview controller

The evaluation criteria P, MW and PW represent three independent driver "moods". They are calculated as follows:

- *Maximizing lateral performance, P*

$$J_P = \left(y_{veh} - y_{des}\right)^2 = y_e^2 \tag{22a}$$

$$P = \frac{\dfrac{\sum_1^n J_P}{n}}{\dfrac{\sum_1^n J_{P,reference}}{n}} \tag{22b}$$

y_{veh} is the global lateral position of the vehicle and y_{des} is the global y-coordinate of the desired road. J_p is the cost value of the error between these parameters, which is averaged over n simulation time steps and divided by the average of the reference condition to yield P. The reference condition is defined by the NMS parameters as described in Table 1 and the preview parameters as described in section 6.1. A low value of P indicates a high lateral performance.

- *Minimizing mental workload, MW*

$$J_{MW} = T_{FF,\mathrm{supraspinal}}^{\;2} \tag{23a}$$

$$MW = \frac{\frac{\sum_{1}^{n} J_{MW}}{n}}{\frac{\sum_{1}^{n} J_{MW,reference}}{n}} \tag{23b}$$

Where $T_{FF,supraspinal}$ is the brain signal output from the preview controller added to the muscle spindle feedback; the higher this signal the more the driver has to use his brains to calculate the desired road.

- *Physical workload, PW*

$$J_{PW} = \left(T_{muscle} + T_{co-contraction}\right)^2 \tag{24a}$$

$$PW = \frac{\frac{\sum_{1}^{n} J_{PW}}{n}}{\frac{\sum_{1}^{n} J_{PW,reference}}{n}} \tag{24b}$$

In which T_{muscle} is equal to the muscle torque generated in response to the feed forward control actions originating from the brain and $T_{co\text{-}contraction}$ represents the muscle torque needed to co-contract the muscles in order to increase the intrinsic stiffness K_{int} and damping B_{int}. The relation between K_{int} and the muscle torque $T_{co\text{-}contraction}$ is established by Pick and Cole [5] as follows:

$$T_{co-contraction} = e \cdot \left(\frac{K_{\text{int}}}{1.8}\right) \tag{25}$$

This equation describes the co-contraction torque as a function of the realized joint stiffness. The factor *e* represents the percentage of the total time the driver uses co-contraction. *e* is assumed to be 1 in the scenario where a disturbance is applied, i.e. if the driver uses co-contraction, he uses co-contraction the complete duration of the torque disturbance test. During the lane change *e* is smaller than 1 since the driver can preview the areas where thinks he will need co-contraction. One way to estimate the value of *e* during the lane change is by looking at the steering wheel torque applied by the driver during a lane change. By looking at the parts where the absolute value of the torque has a positive derivative, the largest driver interventions are selected. Introducing an error here has probably the biggest consequences and therefore it is assumed that during these parts the driver applies co-contractions. The resulting values for e are displayed in Table 5.

Table 5. Values for e during different scenarios, where e represents the fraction of the total simulation time that co-contraction is applied

	Linear tires, perfect IM	**Linear tires, 2nd order IM**	**Non-linear tires, perfect IM**
Time Factor, e	0.396	0.242	0.388

An average of all three criteria (P, PW and MW) with equal weight factor is introduced as a fourth driver mood, and is called TOT. The value of TOT is calculated by dividing each individual cost criteria by the average value from the reference condition (called "ref" in Table 6), see eq. (26).

$$TOT = P + MW + PW \tag{26}$$

Table 6 shows the effect on the 4 driver moods of changing the 5 driver model parameters of Table 4. This test is repeated 3 times to also see the result of having a 2nd order version of the internal model, driving a vehicle with non-linear tires and driving an understeering vehicle.

Table 6. The cost values of the different driver moods (P, MW, PW and TOT), for two different environments (a lane change and a lane keeping task with 5000 N side force disturbance) and 4 scenarios (the original 11th order internal model with matching vehicle dynamics, a 2nd order internal model while keeping the original vehicle dynamics, the original internal model an the vehicle equipped with non-linear tires, and the original internal model while equipping the vehicle with tires at the front which have half the stiffness of the rear tires). Green and red colored cells indicate that the value is 10% or less and 10 % or more than the reference value respectively. The reference value used for the colored cells changes per scenario.

			Lane change				5000 N Disturbance			
Scenario	**Variable**	**Value**	**P**	**MW**	**PW**	**TOT**	**P**	**MW**	**PW**	**TOT**
Linear tires, perfect Internal Model	$U_{co\text{-}contraction}$	0 = ref	1	1	1	3	1	1	1	3
		0.5	0.8739	0.8088	2.4191	4.1019	0.0228	0.0250	18.1398	18.1877
		1	0.8641	0.785	3.793	5.4433	0.0100	0.0109	35.3043	35.3253
	$u_{spindels}$	0 = ref	1	1	1	3	1	1	1	3
		0.5	0.9389	0.9198	0.9295	2.7884	0.3225	0.3275	1.0715	1.7215
		1	0.9125	0.8704	0.9452	2.7282	0.1649	0.1691	1.1434	1.4775
	T_{prev}	0.05	1.2740	2.8410	2.4167	6.5321	1.1052	1.2586	0.0499	2.4343
		0.2 = ref	1	1	1	3	1	1	1	3
		0.3	0.98339	0.9749	0.9964	2.9548	0.9473	0.9655	0.9594	2.8723
	P_{yaw}	6	1.8553	2.3332	0.5448	4.7334	2.2631	1.6551	0.0557	3.9757
		13 = ref	1	1	1	3	1	1	1	3
		19	0.9702	1.0644	1.2502	3.2847	6.8421	0.9482	0.1064	1.7502
	P_y	1.0	1.2945	0.7401	0.6469	2.6819	1.7368	1	4.6191	2.4520
		1.6 = ref	1	1	1	3	1	1	1	3
		2.2	0.9203	1.5962	0.8586	3.3755	0.6842	1.1200	0.0573	1.8526
Linear tires, 2nd order Internal Model	$U_{co\text{-}contraction}$	0 = ref	0.8221	0.7555	1.4153	2.9933	0.7368	0.6896	0.4665	1.4966
		0.5	0.7103	0.5991	2.8588	4.1686	0.0174	0.0196	17.2655	17.3027
		1	0.7039	0.5765	4.1954	5.4758	0.0076	0.0085	34.4995	34.5156
	$u_{spindels}$	0 = ref	0.8221	0.7555	1.4153	2.9933	0.7368	0.6896	0.4665	1.4966
		0.5	0.7640	0.7143	1.3578	2.8363	0.2607	0.2413	0.1226	0.6287
		1	0.7420	0.6642	1.4066	2.8131	0.1358	0.1421	0.2667	0.5448
	T_{prev}	0.05	Uncontr.	Uncontr.	Uncontr.	Uncontr.	0.8421	6.6379	5.1750	12.6693
		0.2 = ref	0.8221	0.7555	1.4153	2.9933	0.7368	0.6896	0.4665	1.4966
		0.3	0.7562	0.4355	0.6082	1.7999	0.7368	0.6724	0.0394	1.4220
	P_{yaw}	6	1.7313	2.4663	2.1080	6.3056	1	0.8103	0.0486	1.8655
		13 = ref	0.8221	0.7555	1.4153	2.9933	0.7368	0.6896	0.4665	1.4966
		19	0.8324	0.6070	1.4504	2.8901	0.6315	0.6724	0.0468	1.3269
	P_y	1	1.1177	0.6077	1.2460	2.9717	1.5263	0.6896	0.0440	2.2749
		1.6 = ref	0.8221	0.7555	1.4100	2.9933	0.7368	0.6896	0.4665	1.4966
		2.2	0.6712	0.9563	1.6664	3.2940	0.4331	0.6896	0.0487	1.1785

Table 6 - continued -

Scenario	Variable	Value	Lane change P	Lane change MW	Lane change PW	Lane change TOT	5000 N Disturbance P	5000 N Disturbance MW	5000 N Disturbance PW	5000 N Disturbance TOT
Non-linear tires, perfect Internal Model	$U_{co\text{-}contraction}$	0 = ref	0.2857	0.6166	0.7227	1.6253	0.7368	0.9137	0.1998	1.8656
		0.5	0.2198	0.4141	2.1981	2.8325	0.0178	0.0228	17.4152	17.4560
		1	0.2169	0.4022	3.5449	4.1640	0.0078	0.0099	34.6513	34.6691
	$u_{spindels}$	0 = ref	0.2857	0.6166	0.7227	1.6253	0.7368	0.9137	0.1998	1.8656
		0.5	0.2423	0.4917	0.7590	1.4930	0.2515	0.2931	0.2632	0.8108
		1	0.2340	0.4642	0.7932	1.4914	0.1295	0.1684	0.3336	0.6316
	T_{prev}	0.05	1.2440	5.0361	4.6128	10.8933	0.7894	0.9827	0.0433	1.8391
		0.2 = ref	0.2857	0.6166	0.7227	1.6253	0.7368	0.9137	0.1998	1.8656
		0.3	0.2711	0.6040	0.7200	1.5960	0.6842	0.9482	0.2256	1.8581
	P_{yaw}	6	Uncontr.	Uncontr.	Uncontr.	Uncontr.	1.1052	1.0172	0.0527	2.1709
		13 = ref	0.2857	0.6166	0.7227	1.6253	0.7368	0.9137	0.1998	1.8656
		19	0.2427	0.6430	1.4262	2.3130	0.5789	0.8793	0.2786	1.7397
	P_y	1	0.2486	0.3822	2.0654	2.6968	1.4736	0.9137	0.0565	2.4207
		1.6 = ref	0.2857	0.6166	0.7227	1.6253	0.7368	0.9137	0.1998	1.8656
		2.2	0.4860	2.0783	1.9134	4.4779	0.4661	0.9310	0.0697	1.4598
Linear tires, perfect Internal Model, front tire stiffness*0.5	$U_{co\text{-}contraction}$	0 = ref	2.4616	1.8543	0.8497	5.1655	1	0.9137	1	2.2502
		0.5	2.4150	1.7272	2.2176	6.3604	0.0231	0.0216	51.5385	17.5898
		1	2.4162	1.7244	3.6130	7.7539	0.0101	0.0095	102.1409	34.7908
	$u_{spindels}$	0 = ref	2.4616	1.8543	0.8497	5.1655	1	0.9137	1	2.2502
		0.5	2.4367	1.7838	0.8627	5.0833	0.3368	0.2931	1.2295	1.0547
		1	2.4294	1.7591	0.8710	5.0592	0.1737	0.1570	1.5680	0.8646
	T_{prev}	0.05	2.3234	4.3525	2.3480	8.7018	1.3157	1.2931	0.1181	2.6224
		0.2 = ref	2.4616	1.8543	0.8497	5.1655	1	0.9137	1	2.2502
		0.3	2.6018	1.7523	0.7923	5.1465	0.9473	0.8275	1.6799	2.3468
	P_{yaw}	6	2.6971	2.5357	0.4339	5.6665	2.3157	1.500	0.1302	3.8576
		13 = ref	2.4616	1.8543	0.8497	5.1655	1	0.9137	1	2.2502
		19	2.0708	2.1778	1.5761	5.8247	0.7368	0.8620	0.9079	1.8819
	P_y	1	3.2344	1.4362	0.7027	5.3738	1.7368	0.8448	0.1501	2.6447
		1.6 = ref	2.4616	1.8543	0.8497	5.1655	1	0.9137	1	2.2502
		2.2	1.8207	2.4580	0.9626	5.2420	0.7368	1.0862	0.2000	1.8837

In general, the best performance is achieved with a high gain on the lateral error and with maximum co-contraction. The lowest mental workload is seen to occur in case the preview gains are low and the lowest physical workload can be found when co-contraction is applied and the preview gains are low. The best overall performance seems to be when the spindle gains are high and the preview gain is moderate. The table furthermore does not reveal unrealistic definitions of P, MW and PW.

6.6. Parameter optimization

In this section the optimal value of each of the 5 parameters displayed in Table 4 is determined by using a bounded optimization algorithm. The driver model parameters of Table 1 are used, with u_{spin} = u_{cc} = 0.5. Besides the 2 environment conditions already used in Table 6 (the lane change and a 5000 N disturbance of Figure 22 during a lane keeping), a third condition is added. A high frequency force disturbance of 5000 N at 8 Hz was simulated, see Figure 30, to investigate if the spindle reflex gain actually has to be lowered due to the time lag on the response as was mentioned in section 4.1.

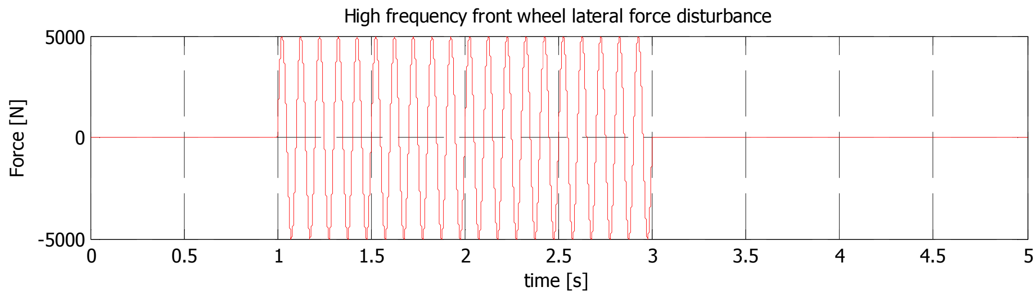

Figure 30. The "high frequency" disturbance. From 1 – 3 seconds a sinusoid with a frequency of 8 Hz and amplitude of 5000 N is applied as a disturbance to the front tires.

The optimal co-contraction u_{cc} level is found in Figure 31. As expected, the optimal value is zero for minimizing PW for all scenarios. The optimal value of u_{cc} for the total workload is zero for the lane change because very little improvement in MW and P is achieved by using full co-contraction whereas the PW does significantly increase.

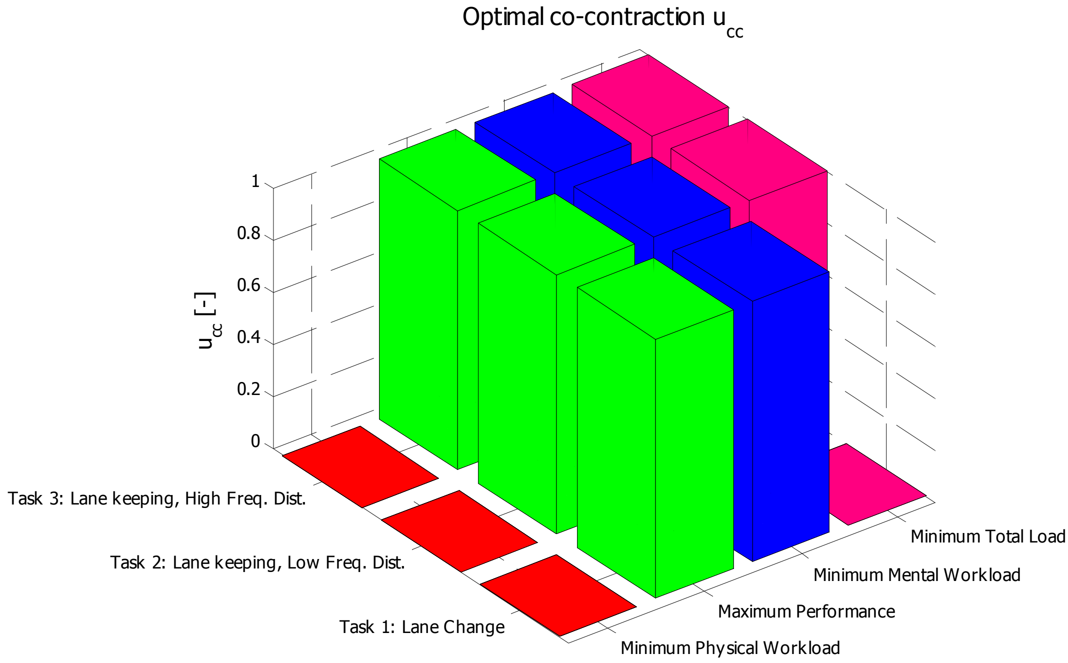

Figure 31. Optimization of the co-contraction level for different moods (minimize physical workload, maximize path tracking performance, minimize mental workload and minimize the average of the three preceding moods) and environment conditions (an ISO 3888-1 double lane change, a lane keeping with a disturbance as displayed in Figure 22, and a lane keeping with a disturbance as displayed in Figure 31)

The optimization result of the spindle gain (Figure 32) largely resembles the co-contraction optimization; however the high frequency disturbance case is indeed different. Due to the time delay of the spindle actions, the high frequency disturbance causes the vehicle to become less controllable, resulting in an optimum value of u_{spin} of 0 for the mental workload minimization and an optimum value of 0.52 for the performance minimization.

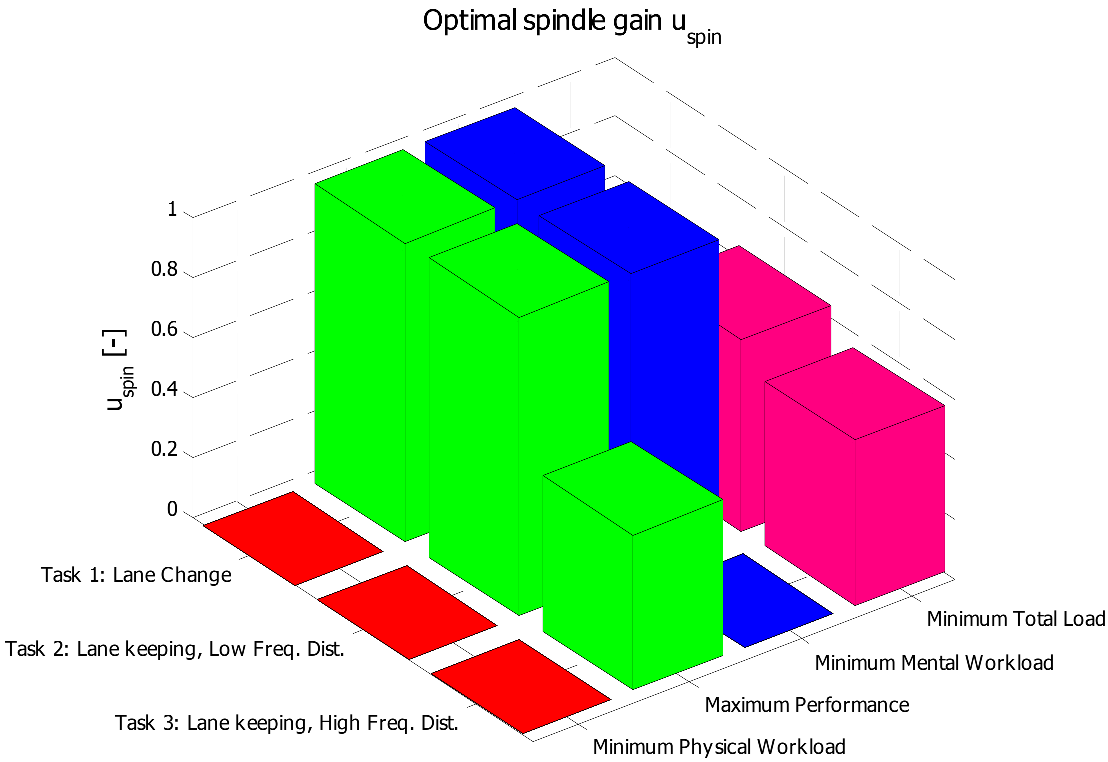

Figure 32. Optimization of the spindle scaling gain u_{spin} for different moods (minimize physical workload, maximize path tracking performance, minimize mental workload and minimize the average of the three preceding moods) and environment conditions (an ISO 3888-1 double lane change, a lane keeping with a disturbance as displayed in Figure 22, and a lane keeping with a disturbance as displayed in Figure 31)

The next optimization was done on the lateral error gain. The scenarios with disturbances require the lateral error gain to be very low, as can be seen in Figure 33. Due to the time delay between the error and subsequent action a large gain quickly leads to instability. During the lane change a high lateral error gain is good for tracking performance. This is also the case for the minimization of the physical workload. The mental workload has its lowest value if no brain signal is generated at all, and therefore the optimal lateral error gain is zero in this case.

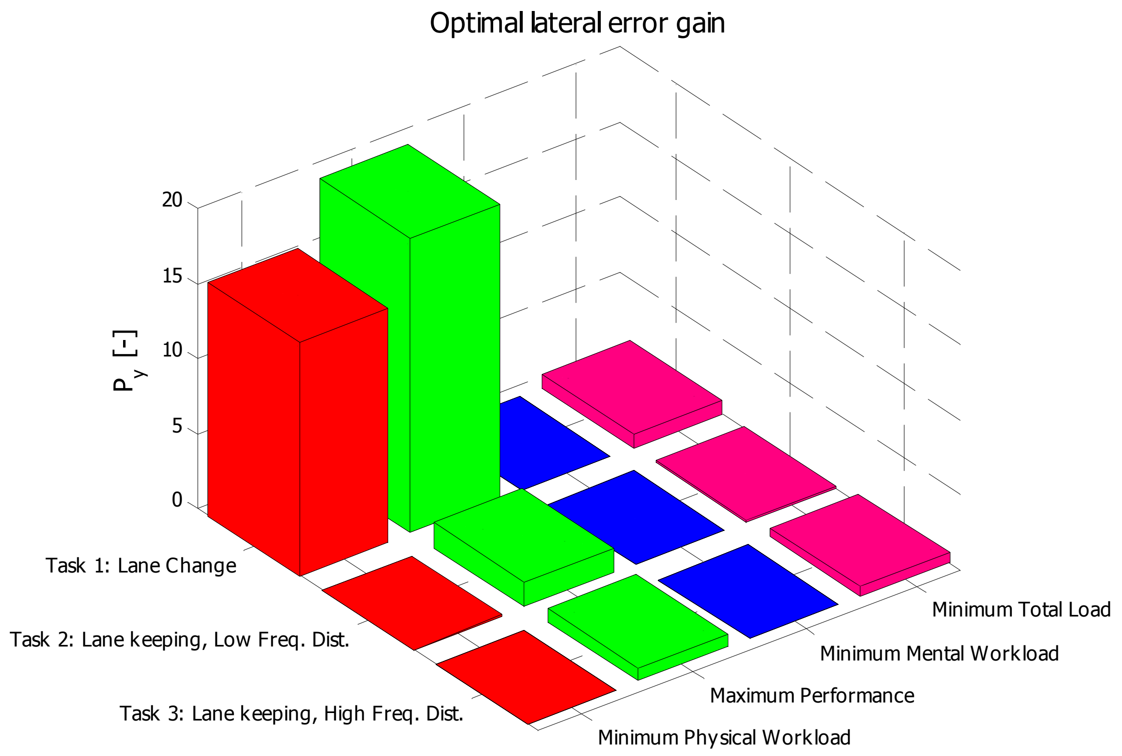

Figure 33. Optimization of the lateral error gain for different moods (minimize physical workload, maximize path tracking performance, minimize mental workload and minimize the average of the three preceding moods) and environment conditions (an ISO 3888-1 double lane change, a lane keeping with a disturbance as displayed in Figure 22, and a lane keeping with a disturbance as displayed in Figure 31)

The optimal yaw angle error gain (Figure 34) is similar to the lateral error gain plot. Comparing the absolute values of the lateral error gain and yaw angle error gain during low frequency disturbances, it appears to be more efficient to steer the vehicle according to the yaw angle gain instead of the lateral error gain. This is also believed to be a driving technique used by experienced drivers.

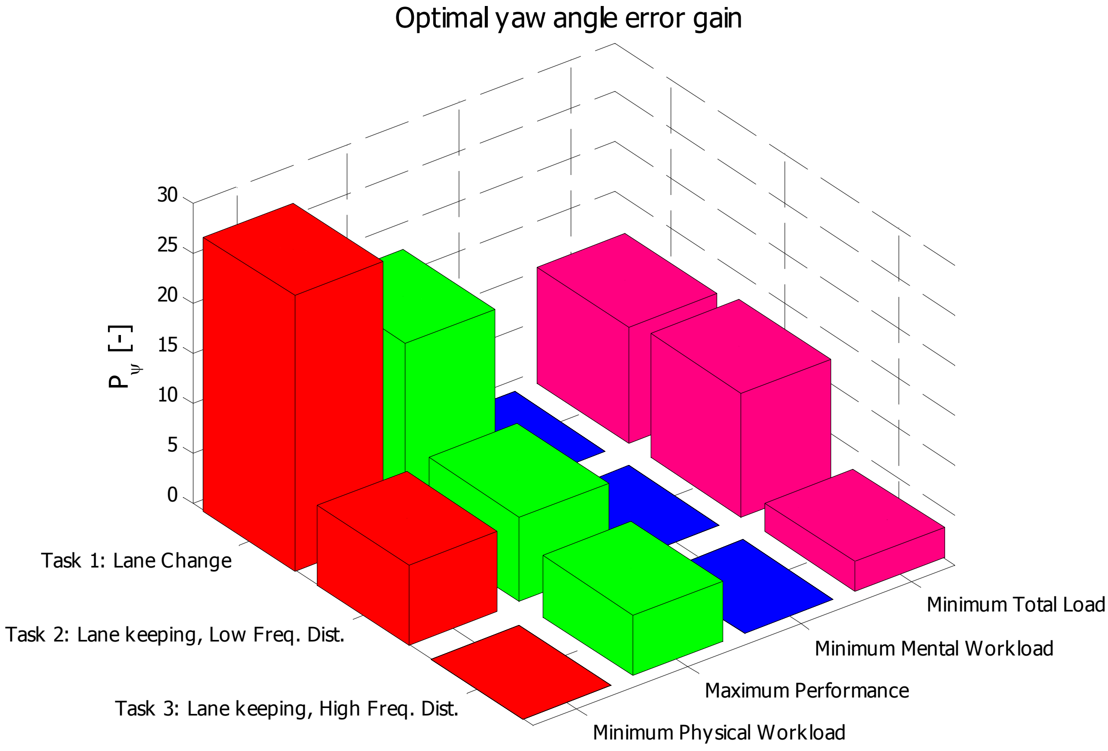

Figure 34. Optimization of the yaw angle error gain for different moods (minimize physical workload, maximize path tracking performance, minimize mental workload and minimize the average of the three preceding moods) and environment conditions (an ISO 3888-1 double lane change, a lane keeping with a disturbance as displayed in Figure 22, and a lane keeping with a disturbance as displayed in Figure 31)

The final optimization plot (Figure 35) pictures the optimal look-ahead time of the preview controller. During the lane change it is beneficial to look far ahead, but since the previewed error will also be larger, the physical workload prefers a short look-ahead time. This effect is less profound when multiple preview points would be used. The same applies to the disturbances: as already seen in the preceding two plots, the gain on the lateral and yaw angle error should not be too large.

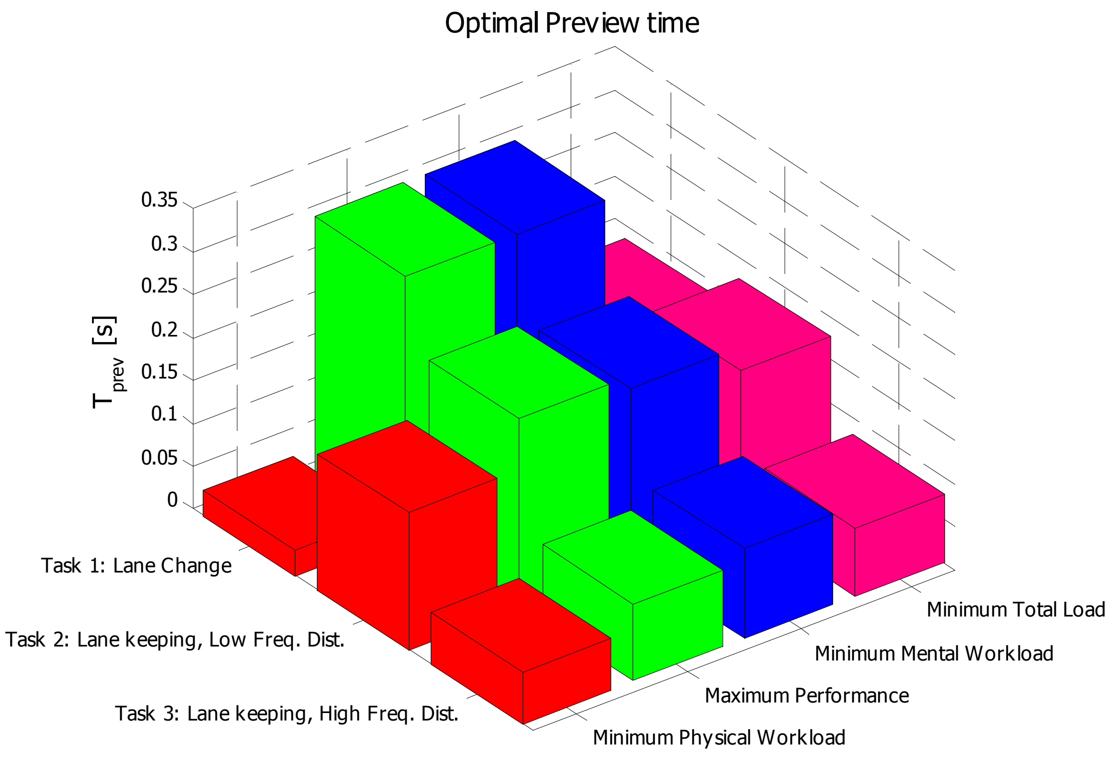

Figure 35. Optimization of the preview time for different moods (minimize physical workload, maximize path tracking performance, minimize mental workload and minimize the average of the three preceding moods) and environment conditions (an ISO 3888-1 double lane change, a lane keeping with a disturbance as displayed in Figure 22, and a lane keeping with a disturbance as displayed in Figure 31)

7. An application: Using the driver model to design a steering system

In chapter 5 the importance of adding a NMS structure to a driver model was shown, which was supported by simulation findings in section 6.2. In section 6.5 it was shown that the selection of realistic driver model parameters depends on the driver's mood and the environment condition. Therefore it is hypothesized that the steering system configuration as desired by the driver also changes according to his mood and the environment condition. In this chapter it is shown that this is indeed true and a first step can be taken to focus more on the driver when defining the requirements for the steering system design.

Three steering system parameters from the system described in section 5.2.1 are optimized: the power steering gain, the steering ratio and the steering wheel damping (encircled in Figure 36). The optimal value is calculated for the same 4 driver moods from section 6.5, but the environment conditions are altered. Since current steering systems often incorporate a velocity dependency, the lane change is conducted both at 80 km/h and at 20 km/h, as well as the lane keeping scenario with the force disturbance of 5000 N (refer to Figure 22). For reasons of brevity the high frequency disturbance is omitted in this section.

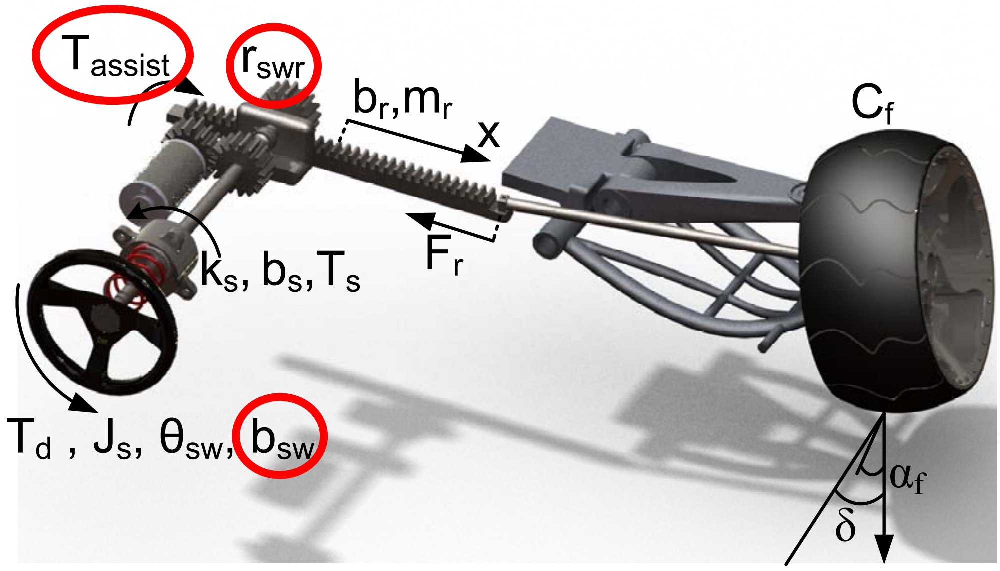

Figure 36. The steering system lay-out, with the red circles indicating the three parameters that are subjected to an optimization routine in this chapter (the power assist, T_{assist}, the steering ratio, r_{swr}, and the steering wheel damping, b_{sw}). Figure repeated from section 5.2.1, all symbols and their values are listed there

First the optimal power steering gain (T_{assist} in Figure 36 and eq. (18)) is calculated by allowing it to change between 0 and 10; which are values encountered in current steering systems. The driver's internal model is constantly adapted to the different power steering gains. The optimization result is pictured in Figure 37, where it can be seen that in almost all cases the maximum gain is beneficial. Since the driver behaves optimal (no internal noise and an internal model that perfectly matches the NMS and vehicle dynamics), the high gains in the simulation do not lead to instability as would be in real life. When in the future the internal model is validated with real drivers and noise sources are found, these optimizations should be redone. A negative value is assigned to the maximum performance objective during the lane change at 20 km/h, this is to indicate that the value for the performance metric is equal for all power steering gains. Only during the lane change at 80 km/h the physical workload minimization demands the power steering gain to be as low as possible. This can be explained by looking at Figure 38, where the bode plots of two internal models are pictured.

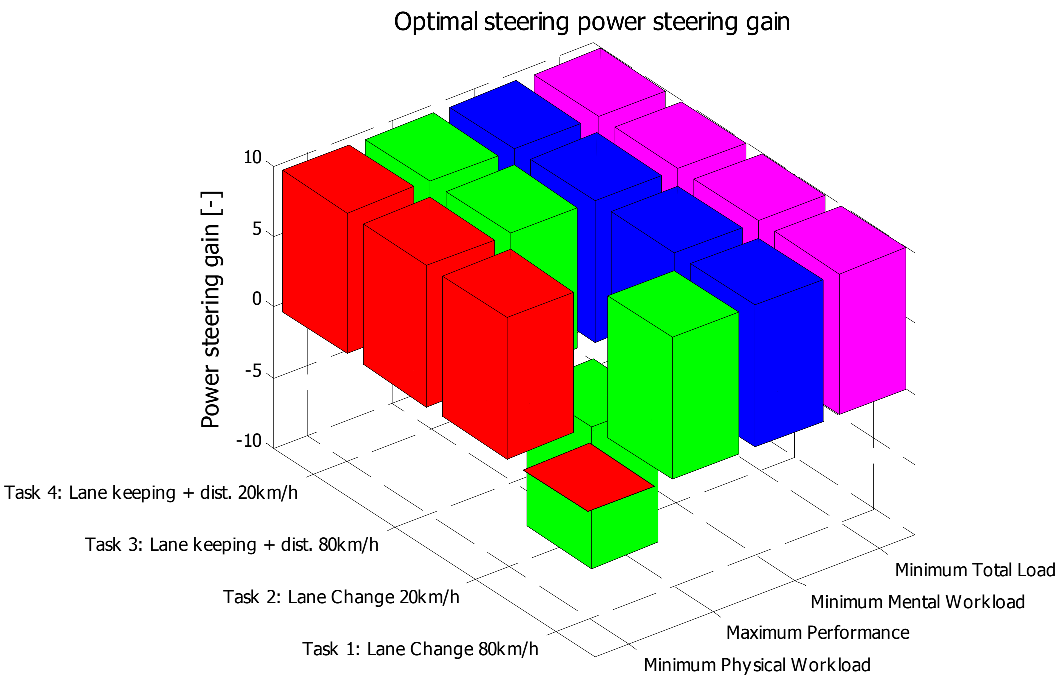

Figure 37. Optimal power steering gain for different moods (minimize physical workload, maximize path tracking performance, minimize mental workload and minimize the average of the three preceding moods) and environment conditions (an ISO 3888-1 double lane change at 20 km/h and 80 km/h and a lane keeping with a disturbance as displayed in Figure 22 with 20 km/h and 80 km/h. Negative values indicate that the cost value for that particular mood and environment condition is equal for all different power steering gains

The green line represents the internal model with no power steering gain and the red line indicates the internal model response if the power steering gain is set to 10 Nm/Nm. Since the lane change at 80 km/h is a very dynamic steering process, the internal model output is never lower than 2 rad/s. In this area the high power steering gain requires more muscle torque due to the lower damping (at 1 – 3 rad/s). It is interesting to see that the power steering gain in this system only helps to decrease physical workload at low frequencies. Future evaluations with real systems and/or improved steering system models should point out if this is generally the case. If so, the power steering system should be redesigned.

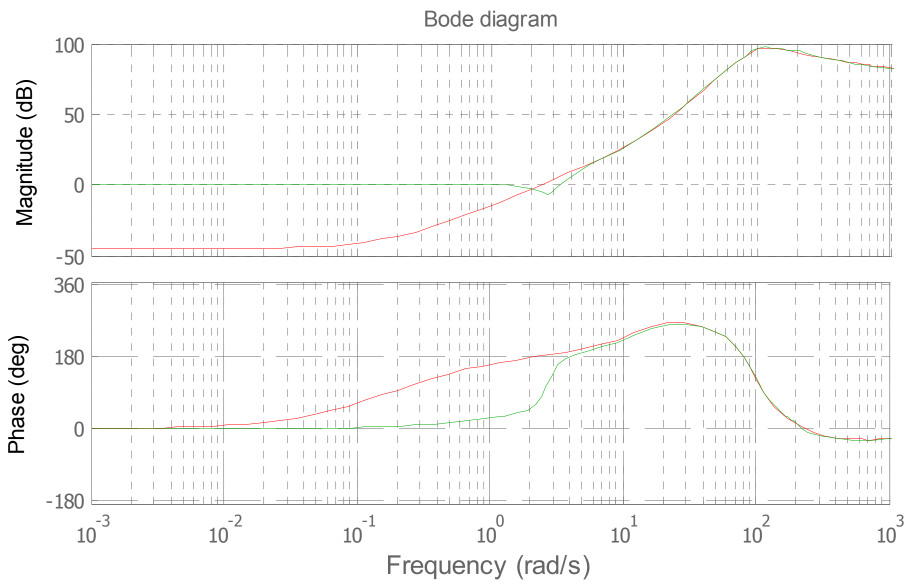

Figure 38. Bode diagram of two internal models; green = no power steering gain; red = a power steering gain of 10 Nm/Nm

The next parameter optimization is carried out on the steering wheel damping (b_{sw} in Figure 36 and eq. (16)). The damping value is allowed to change between 0 and 1 Nm/rad/s. The results are visualized in Figure 39. In the scenarios without disturbance the minimum physical workload could obviously be found when no damping was applied. The performance and mental workload were not affected by a change in damping, since the internal model could completely compensate for the effect. In the disturbed cases however, damping was desired because it absorbs part of the disturbance. This is also true at 80 km/h, however the mental and physical workload start to suffer from the extra muscle torque needed to steer the vehicle. In general, it seems wise to implement a very low steering wheel damping and let the damping of disturbance be done by the driver's reflexes.

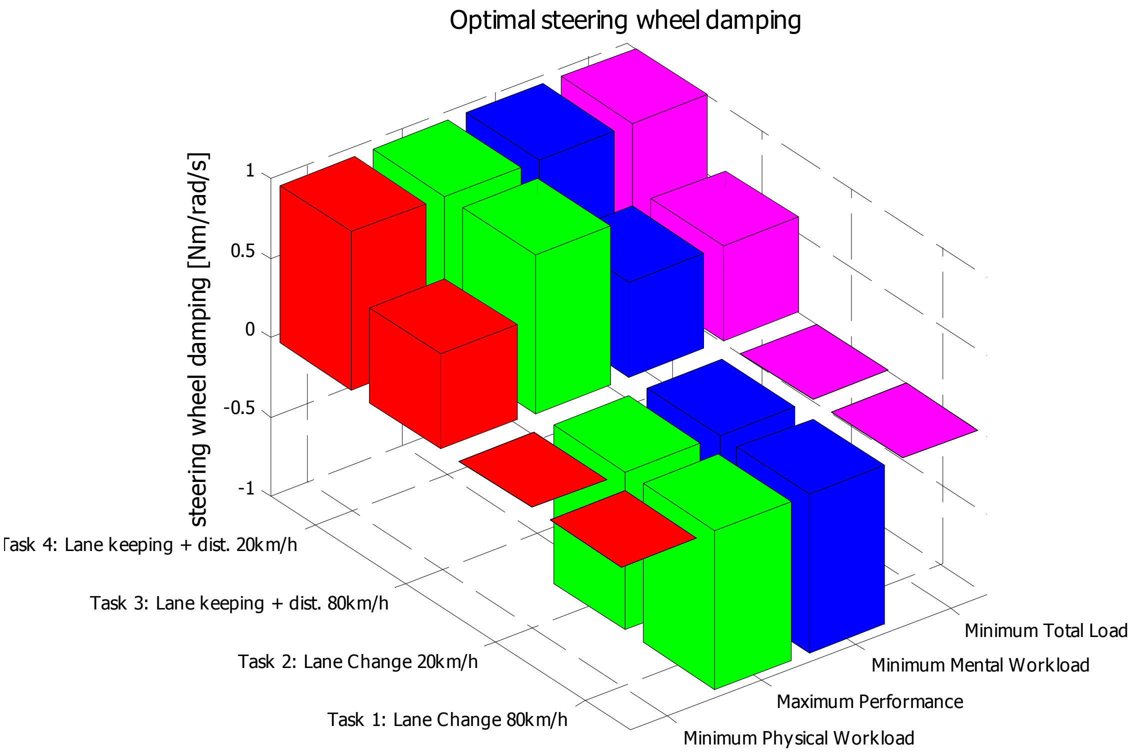

Figure 39. Optimal steering wheel damping for different moods (minimize physical workload, maximize path tracking performance, minimize mental workload and minimize the average of the three preceding moods) and environment conditions (an ISO 3888-1 double lane change at 20 km/h and 80 km/h and a lane keeping with a disturbance as displayed in Figure 22 with 20 km/h and 80 km/h. Negative values indicate that the cost value for that particular mood and environment condition is equal for all different steering wheel damping values

The final parameter to be varied is the steering ratio (i_{sw} in Figure 36 and eq. (20)). The steering ratio can be selected between 1:1 and 1:30). Again, it is assumed that the driver driving a vehicle equipped with a different steering ratio completely adapted to it. The results are pictured in Figure 40. In the disturbed scenarios a high steering ratio is beneficial due to the lower forces needed to counteract the disturbance. The subsequent higher steering wheel angle deviation provokes a higher torque from the intrinsic dynamics and reflexes which respond to changes in position and velocity. In reality, at very high steering wheel angles the disturbance cannot be sensed anymore by the driver, which will not trigger the fast reflexes of the driver and subsequently the performance drops. Also, in the model the inconvenience of steering to an angle more than the hands can achieve without changing position is not modeled. At large steering ratios this will become an issue. The lane change at 20 km/h prefers a low ratio, probably because of the lower steering wheel speeds and subsequent lower energy loss due to damping. At 80 km/h the optimal ratio is somewhat higher; at steering ratios below 1: 4 the muscle torque approaches the muscle torque limit set in Table 1: 50 Nm. The results comply with the variable steering ratio steering systems on the market, which often have a lower ratio at speeds within urban limits, albeit that in our simulations all optimal ratios are quite low. Comparison to steering systems on the market should point out if this is realistic.

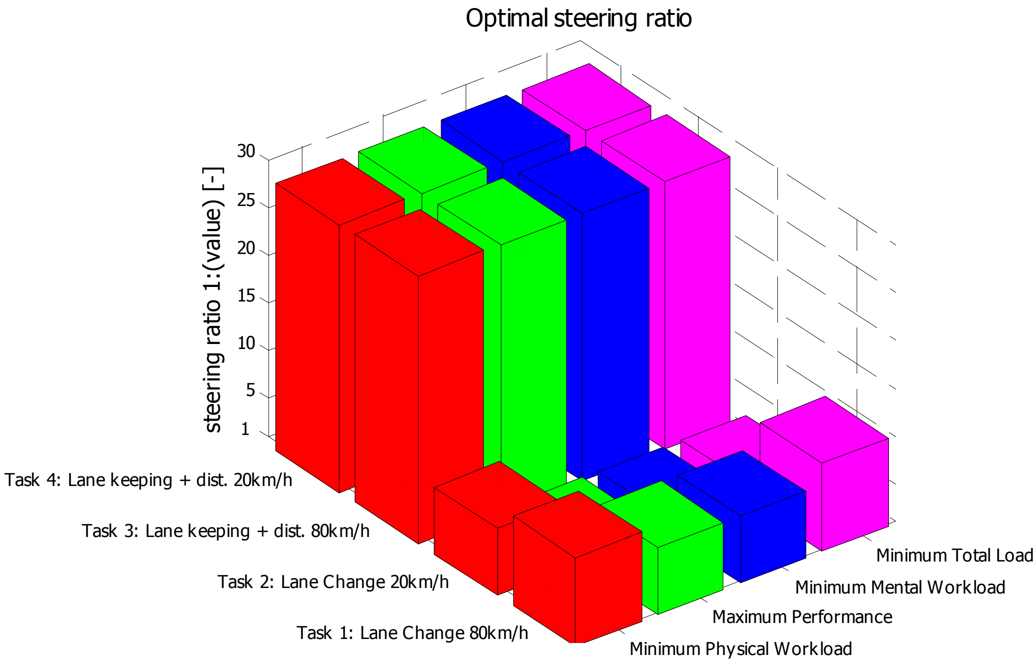

Figure 40. Optimal steering ratios for different moods (minimize physical workload, maximize path tracking performance, minimize mental workload and minimize the average of the three preceding moods) and environment conditions (an ISO 3888-1 double lane change at 20 km/h and 80 km/h and a lane keeping with a disturbance as displayed in Figure 22 with 20 km/h and 80 km/h. Negative values indicate that the cost value for that particular mood and environment condition is equal for all different steering wheel ratios

Already in these 4 arbitrarily chosen scenarios the driver requires very different optimal power steering gains, steering wheel dampings and steering ratios. It was found that in accordance with commercial steering systems it is beneficial to have a higher steering ratio when the vehicle speed is increased. Also, it was noticed that a high power steering gain leads to increased physical workload during dynamics maneuvers due to the lower overall damping of the steering system.

In this chapter it became also clear that the analyses probably can be improved by expanding the current steering system model, e.g. by incorporating compliance. Also, the driver model needs improvement by modeling realistic inaccurate driver control behavior and accounting for the effect of having to relocate your hands for large steering angles. However since modern steering systems in production vehicles (e.g. BMWs mechatronical Active Steering or Mercedes Benz’ mechanical ActivRak™) are not taking into account different driver moods and different disturbances and they do not have for instance adaptive wheel damping, it is clear that current steering system design can be improved.

8. Discussion

Designing steering systems which improve safety and comfort requires focus on the needs, wants and limitations of the driver. In industry steering system requirements imposed by the driver are often defined by a certain "steering feel". Many different steering feels have been proposed (e.g. [28][39][40]), describing different optimal relations between the torque applied on the steering wheel and the resulting angle. Although the researchers generally acknowledge that the desired steering feel is also dependent on the driver, few useful tangible requirements can be found that tie the steering feel to the driver characteristics or moods. Traditional design methods rely heavily on evaluations by expert drivers in a time consuming trial-and-error process. Evaluations with real cars is constrained by a very limited adjustment range of the steering system. Additionally, issues like repeatability; cost and time nominate the use of moving base driving simulators. Still, they cannot provide a completely realistic driving feel because of the simplified vehicle dynamics, suboptimal graphics and the necessary vestibular stimulants during severe cornering situations due to actuator stroke limits. Fixed base simulators clearly do not cope with the latter problem but they do not provide the driver with vestibular motion cues.

Although moving base driving simulators save time and cost because of the evaluation being possible at an early point in the design phase, they still have to deal with the subjective evaluation process. As outlined in this thesis, substituting the driver by a driver model can offer several advantages, summarized as:

- The driver model serves as an objective performance metric.
- Optimization of driver model parameters can predict the adaptive, driver dependent driving style (see chapter 6), according to different:
    - Steering systems
    - Driving conditions
    - Driving tasks
    - Available cues
    - Quality of the cues
    - Physical NMS limitations
    - Disturbances
    - Etcetera
- The steering feel metric can be substituted by a driver model which contains measurable and quantifiable metrics such as mental or physical workload, which is adaptive to environments and can model different driver experience levels.
- Since the vehicle and the driver are replaced by a computer model, optimization routines can be implemented to find the optimal steering system design (see chapter 7). The evaluation can directly be done by the computer, saving considerable time.

Obviously, the driver model cannot completely substitute real drivers in the evaluation process. One of the main reasons is the lack of current driver models to account for the response to vestibular and kinesthetic cues. But it will be used as a guideline that will speed up the design process.

8.1. The NMS driver model

Steering system evaluation requires a driver model which is able to:

- Follow a desired road trajectory
- Describe the force interaction between the driver and steering wheel
- Steer large angles
- Model the limitations of the driver as a controller
- Describe the adaptive behavior of the driver
- Model different driving styles

The driver model of Abbink [2] building on a NMS arm model of de Vlugt [9] can potentially fulfill these requirements; however it is developed and identified only for stationary conditions where the desired joint position remains constant. In Figure 41 the red blocks (except for the path following controller) derive from this model. The path following controller is a single point preview model [26] which estimates the vehicle future position using a 2 DOF linear vehicle model. The steering dynamics block contains a 2 DOF steering system, which is connected to a linear 2 DOF vehicle dynamics model. In order to test the original model of Abbink [2] in case large steering angles are desired, the response of the model was monitored while a desired steering wheel angle of 1 rad was applied to the input. The final steering angle reached was only 0.15 rad. Two major model adjustments over the original model were implemented to make the realized angle follow the desired angle. Those two adjustments resulted in the addition of the green colored parts in Figure 41.

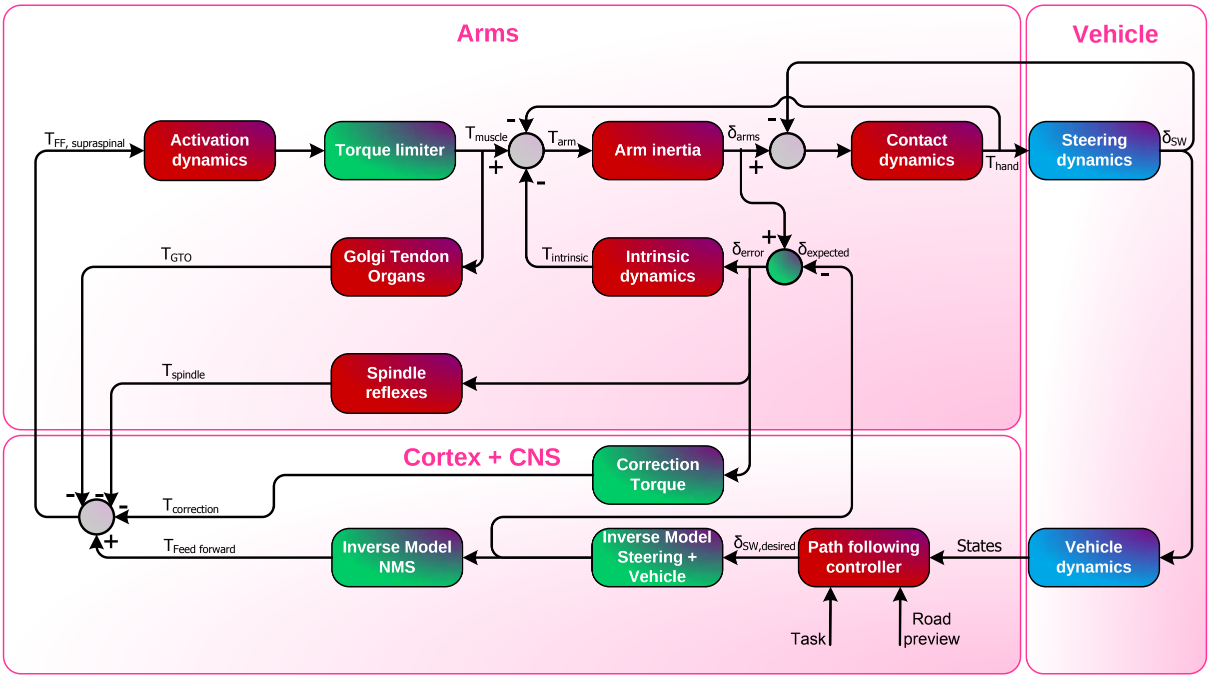

Figure 41. The new NMS driver model, green parts are newly introduced parts compared to the original driver model of Abbink [2] building on NMS arm models of de Vlugt [9] (equal to Figure 13)

The first adjustment was made by introducing a "moving reference" steering angle position. For straight line lane keeping scenarios the original model with its fixed reference works perfectly, whereas for scenarios where the desired steering angle is constantly changing (all other scenarios except lane keeping), a moving reference position is needed. Otherwise the driver counteracts his own intrinsic limb stiffness and damping (the "intrinsic dynamics") and muscle spindle reflexes, which try to push the steering wheel position back to the fixed reference position. This moving reference position represents the expected steering wheel position. If the driver has an accurate representation of the vehicle dynamics, the expected and real steering wheel position will be quite similar and his reflexes and intrinsic dynamics will not come into play. However if the driver has a bad representation of the vehicle, he will command too much or too little force and the steering wheel will not follow the desired steering wheel angle, which is counteracted by his intrinsic dynamics and reflexes. The internal representation of the driver's arms dynamics and the system he controls is modeled by the inverse internal model, which is discussed next.

The driver turns the steering wheel by commanding a muscle force from the brain. The exact amount of force needed to achieve the desired steering angle depends on the dynamics of his NMS and the vehicle (with steering system). The knowledge of these two system gained by the driver is modeled in two blocks: the inverse model of the NMS and the inverse model of the vehicle including the steering column. Simulations showed that only after the moving reference and the inverse internal models were both implemented, the model could accurately follow the desired steering wheel angle in rapid lane changes.

Since the internal inverse models invert the dynamics of the NMS and vehicle, the output of this model at high frequencies can be very high. Thus, a torque limiter saturating the output torque to 50 Nm was implemented. Part of this maximum available torque will also be used for co-contraction. In this report a relation established by Pick [5] is used to rate co-contraction effort (the torque needed is the resulting intrinsic stiffness divided by 1.8), but since the parameters of the rest of the driver model are obtained using different evaluation methods (Van der Helm [27]) further investigation is required to confirm this relation. Considering a Hill-type model, the torque limit could also be dependent on the speed and position of the muscles. Also, adding a series element (SE) and parallel Hill type element (PE) will limit the bandwidth of the NMS dynamics even further. Again, it has to be experimentally investigated how the Hill characteristics can be integrated in the driver model.

A simulation was done with a preview model and the new NMS model in section 6.2 where the driver was keeping the middle of a straight road, when suddenly a side wind force of 5000 N was applied. Since the preview model can only notice the change in vehicle trajectory by the slow visual channel (0.16 seconds in this case), the vehicle was seen to drift 38 cm from the center and only very slowly able to stabilize the vehicle again (see Figure 23). However, the new model incorporates quick responses from the intrinsic dynamics and the muscle spindle reflexes (only a 28 ms delay), which results in a vehicle drift of only 8 cm from the road center. With full co-contraction the wind disturbance had hardly any effect on the vehicle trajectory.

A subsequent simulation was conducted to compare the preview model with the new NMS model. In this case no disturbance was applied, but both models had to track a double lane change trajectory (Figure 21). As expected, the resulting vehicle trajectories were the equal. Concluding that in this scenario the user could just as well select the conventional preview model is not true. In this case the new model still has two main advantages over the preview model. The first advantage is that the new model incorporates physical limits. If the lane change would be conducted at a higher speed (and corresponding higher required muscle forces) the new model would eventually show a different response compared to the preview model. The second advantage is that the new model contains an inverse internal model.

Besides physical limitations or erroneous steering angle calculations, the internal inverse model is a third source where possible control disabilities of the human derive from. Finally, preview models do not model muscle forces, which are needed to evaluate the response of the driver on different steering system designs. These muscle forces are used as a measure for the physical workload during driving; one of the key judgment parameters for evaluating vehicular system designs in the modeling phase.

To get a feel of how accurately the internal model should match with the real dynamics before the driver loses control of his vehicle three analyses were done in section 6.2.

- In the first case the 11th order accurate internal steering system and vehicle model was reduced in order, by replacing it with a 2nd order model. This process maintained the functional integrity and only very minor differences were noticed. It was not until the internal model was replaced by a zero order (spring) representation that the driver model failed to complete the lane change maneuver.

- In the second case the linear tires model of the vehicle was replaced by non-linear tires, which was not accounted for in the internal model. Differences in path tracking performance were noticeable, but the driver could maintain the vehicle path within a range of one meter.

- Thirdly, the tire stiffness ratio between front and rear was changed, again without the driver being aware of this change. Only very low rear tire stiffness caused the driver to lose control of the vehicle.

It is clear that the performance of the driver depends on the accuracy of his internal model, but apparently the driver can control the vehicle with an internal model that can differ substantially from the real vehicle dynamics. In the latter case the reflexes and co-contraction play a very important role. Further research is needed to determine how the driver learns this model, what levels of accuracy he can achieve, how quick he learns, which factors are important in this learning process and to which extent the driver can cope with non-linear dynamics.

When the vehicle suddenly changes its dynamic behavior (e.g. due to a sudden constant side wind), the internal model should be adjusted to compensate for this. As stated above, this learning process still needs to be investigated, but to temporarily compensate for a mismatch between the real and internal model, a simple controlling feature was added that adjusts the output torque command of the internal model. In case the desired steering angle differs from the realized steering angle for more than 0.5 seconds a PID controller adjusts the muscle torque. In chapter 5 this system proved its value when a sudden side force disturbance was applied during a lane keeping task; however validation is required here.

As is the accuracy of the internal model important, so is the input to this model: the desired steering wheel angle. The angle is calculated by the preview model, which is represented by a single point preview in this report. At 80 km/h, the path tracking accuracy in the double lane change showed to be low for this controller. To improve the path tracking, extra preview points should be added and the steering angle should be allowed to change during the preview calculation process. Ungoren [24] developed such a model based on the Macadam model [3]. It is also desirable to have a model capable of simulating a "race line" trough tight corners and modeling longitudinal driver control (brake and throttle). The latter is important since during heavy cornering the tires can be well at their lateral friction limit. A longitudinal gas- or brake torque decreases the lateral friction limit. Macadam developed the UMTRI model [23] to fulfill these requirements, which has been implemented in commercial software packages. In this UMTRI model (and many other models) the future vehicle path is predicted by using a simple, often 2 DOF vehicle model. This report enables the improvement of the preview path prediction of the vehicle by connecting a (simplified) NMS driver to the vehicle model.

It can be concluded from the simulations in this report that the performance of the driver during severe cornering is mainly depending on the path planning, the vehicle path tracking error control and the inverse internal model. In case the latter two induce an error, the feedback parts (the co-contraction level and the spindle gains) determine the resulting performance. Feedback in the model is received both visually or haptic (via the steering wheel). The haptic feedback enables the reflexes and intrinsic dynamics to compensate for disturbances. The visual feedback is used by the vehicle error controller to adjust the desired steering angle or by the correction torque block to adjust the desired muscle torque. The haptic feedback parts (intrinsic dynamics and spindle reflexes) can be determined for instance by using the identification methods developed by van der Helm [27], the visual feedback path contains many parts that are much harder to validate or identify. For example the internal model, the path error controller and the path planning parts act in series and hence cannot be validated independently. Sophisticated validation methods need to be developed to get a realistic representation of these parts.

The NMS parameters are identified for different steady-state tasks [2][9][29], where the environment is kept constant. Since driving during every day life contains numerous steady-state tasks, identification is a very labourous process (and almost impossible for parameters in the visual feedback part, see above). Therefore in this report the driver model itself is used to determine the optimal parameter values, which at the same time will show that the new driver model is able to model adaptive driver behavior. It was hypothesized that the parameters are dependent on the driving task and the driver mood. The different moods selected are:

- Minimizing physical workload,
- Minimizing mental workload,
- Maximizing path tracking performance.

And the different environment conditions selected were:

- Lane keeping with a disturbance
- Lane keeping with a series of disturbances
- Lane change at 80 km/h

Optimal values of the co-contraction level, muscle spindle gains and preview gains showed to change significantly depending on the above mentioned driver moods and environment condition (lane keeping or lane change). A future step would be to find more objectives and environment conditions that influence the driver's parameter choice.

8.2. Our Vision of the driver NMS model in developing future steering systems

Although finding the different moods of a real driver is rather tedious, we proved in chapter 7 that such knowledge can aid the design of a steering system. Both different environment conditions (lane keeping with a disturbance and a lane change both at 20 km/h and 80 km/h) and driver moods show to have a significant influence on the optimal value of all three design parameters that were tested. Those parameters were the power steering gain, the steering wheel damping and the steering ratio. It would be an interesting comparison if this method yields similar steering system design as recent developments from e.g. BMWs Active steering or Mercedes Benz' ActivRak™ where their design is proprietary and patented. However in commercial steering systems this parameter is usually not adaptive. In chapter 7 the driver model parameters were kept constant, future analyses could benefit from also letting the driver adapt to the new steering system parameter values.

In the future a steering system can be developed identifying the driver objectives and environment conditions real-time and change the steering system parameters accordingly.

Although designing a steering system as described in chapter 7 will improve comfort and safety, the latter can be improved even more. For example the driver can be actively assisted during unsafe situations by providing artificial torque feedback. At the moment, vehicle stability control (VSC) systems maintain safety by acting without notifying the driver. This can cause panic reactions of the driver. VSC systems providing artificial torque feedback which already show good results are lane keeping systems, lane changing systems and haptic gas pedals [2][16][29]. Yuhara [8] is one of the very few on this subject who experimented with artificial torque feedback during severe cornering. He feeds back the predicted yaw rate with a certain gain to aid the driver in providing extra time. However he already indicates himself that this system can be experienced as steering against the driver's intentions. Also it does not actively aid in finding the optimal path to prevent losing control or in case the driver already lost control. Systems that aid in steering the correct path need a map of the road since the steering wheel itself cannot be taken as a reference anymore. This would require complex vehicle systems and infrastructure with similar complex fault rejection systems. Furthermore, modeling of path tracking behavior, once the driver lost control over the vehicle, will also become an issue. However, first the focus is on developing a driver model that is able to model realistic driver behavior such that a optimal new steering system design can be obtained.

9. Conclusion

The new NMS model is based on the NMS model developed over the years in the Delft Biomechanics group (refer to [2][9]). Two major changes were performed in order to cope with large steering angles:

- Since the intrinsic dynamics and reflexes act with respect to a fixed reference point at zero degrees steering wheel angle, the driver has to counteract his own dynamics when applying large steering angles. Therefore a moving reference point was modelled, determined by the driver's desired steering wheel angle.
- The desired steering angle was originally scaled linearly to yield the muscle force command signal. However in case the system to be controlled incorporates first or higher order dynamics, the driver model needs an inverse internal model of this dynamics and his own NMS dynamics in order to command the appropriate muscle force to achieve the desired steering wheel angle.

The NMS model shows clear advantages over a preview model:

- It describes the response of the fast reflexes on steering wheel torque feedback in addition to visual (road trajectory) feedback.
- It is able to model the physical limitations of the driver, such as:
    - The maximum available force
    - The bandwidth
- It uncovers different time-variant driver parameters which partly account for different driving styles. For example:
    - The co-contraction level
    - The muscle spindle position and velocity gains
    - The path planning behaviour
    - The inverse internal model of the dynamics of the driver and the system to be controlled
    - The accuracy of the learnt inverse internal model is an important factor determining driver behaviour.

The NMS model can benefit from the following model extensions:

- Limiting the desired muscle torque as calculated by the inverse internal model.
- Finding the driving factors that determine the value of the time-variant driver parameters
- Finding different noise and disturbance sources, for example motor noise in the muscles or noise on the nervous signals

The preview model has to be studied further for structure validation and the optimization of the parameters. This was beyond the scope of this research for which the primal goal was to introduce a realistic NMS driver model structure combining well established a driver models and NMS system model. The initial goal of this research was successfully met since the proposed structure proved to be an objective performance metric that enables the calculation of optimal steering system parameter values depending on different driving moods (maximum performance, minimum physical workload or minimum mental workload) and driving tasks. We are looking forward to extend this work and see this model describe the desired adaptive behaviour of the steering system to the driver.

10. Recommendations

In addition to the conclusion, the following recommendations are cited:

- Compare the old driver model of de Vlugt [9] to the new model described in chapter 5 by conducting validation experiments. The experiments should either be lane keeping or lane change on a highway, since in these cases the old model is claimed to be valid by Tsoi [29].
- Evaluate the new driver model during more extreme driving situations, while not depending too much on the (not to be validated) preview model part. A circular drive with disturbances for example can be used.
- Replace the single point preview with for example the UMTRI preview model of Macadam [23]. The model of Macadam incorporates:
    - Multi-point preview.
    - Race-line vehicle trajectories trough tight corners.
    - Longitudinal vehicle control; brake- as well as throttle control.
    - Steering angle adjustment possibility during the calculation of the future vehicle position.
- Currently the future vehicle position is calculated without steering system and driver dynamics. If the steering angle adjustment is possible during the future vehicle position (as in Ungoren [24] and Macadam [23]), it is recommended to also connect a (simplified) driver model and steering system model to this vehicle model to improve the vehicle future path estimation.
- The latter point necessitates also a more advanced vehicle dynamics model that at least incorporates:
    - Longitudinal velocity control.
    - Independent wheel rotation.
    - Accurate tire force calculation by:
        - Incorporating non-linear tire characteristics.
        - Modelling the friction circle that defines relation between the lateral and longitudinal force and the resulting maximum available tire force.
        - Modelling accurate normal forces on the tires, which in turn needs at least body roll and pitch modelling.
- Regarding steering system optimization, a more detailed steering system model is needed. It should model:
    - Compliance / play
    - Friction
    - Wear
- The most common disturbances on the steering system should be modelled.
- Also, the internal disturbances and/or noise within the NMS should be found.
- Research and model the path planning behaviour of drivers after they lose control of their vehicle.
- Investigate the importance of adding kinaesthetic cues to the model, as well as the driver's response to force cues applied via the gas and brake pedal.
- Investigate if the proposed Hill-type muscle force and bandwidth limiting features are necessary.
- Define additional driver moods.
- Find out how these moods are affected by the task (lane change, lane keeping, high speed, low speed).

- Investigate which factors determine how drivers learn their internal model, how much time is needed, which accuracy is achieved and if the driver is able to learn non-linear dynamics. Especially focus on the (non-linear) vehicle dynamics parts that are hard to learn and have a great impact on overall stability.
- The current NMS model assumes a perfect “ten to two” grasp of the hands on the steering wheel. The influence of different hand configurations on the final NMS model structure should be examined.
- Investigate how a VSC system can best apply torque feedback to the driver, taking into account his actual driving mood (and therefore driver dynamical behavior).

11. References

[1] D. A. Abbink and M. Mulder, "Exploring the dimensions of haptic feedback support in manual control, J. of Computing and Information Science and Eng. vol. 9, n° 1, 2009.

[2] D. A. Abbink, Neuromuscular Analysis of Haptic Gas Pedal Feedback during Car Following, Ph.D. Thesis, Faculty of Mechanical Engineering, Delft University of Technology, 2006.

[3] C. MacAdam, "An Optimal Preview Control for Linear Systems", J. of Dynamic Systems, Measurement and Control, Trans. of the ASME, Vol. 102, Sept 1980.

[4] A. Kemeny, "Simulation and perception," in Proc. Driving Simul. Conf., Paris, France, Jul. 1999, pp. 21-28.

[5] A. J. Pick and D. J. Cole, "A mathematical model of driver steering control, including neuromuscular dynamics", J. of Dynamic Sys. Measurements and control, Vol. 31, issue 3, 2008.

[6] J. Pick and J. Cole, Dynamic properties of a driver's arms holding a steering Wheel, J. Automobile Engineering, 2007, pp. 1475-1486.

[7] D. T. McRuer, E. S. Krendel, Mathematical models of human pilot behaviour, N.A.T.O. AGARDograph, No. 188, 1974

[8] N. Yuhara, et. al. An advanced steering system with active kinesthetic feedback for handling qualities improvement, Vehicle System Dynamics, 27:5, p. 327 –355, 1997

[9] E. de Vlugt, Identification of spinal reflexes, Ph.D. Thesis, Faculty of Mechanical Engineering, Delft University of Technology, 2004.

[10] A. C. Schouten, E De Vlugt J.J. Van Hilten and F.C.T. Van der Helm, Quantifying proprioceptive reflexes in vivo during postural tasks, IEEE Trans. Biomed. Eng. Vol 55, No 1, January 2008

[11] E. de Vlugt, A.C. Schouten and F.C.T. van der Helm, Quantification of intrinsic and reflexive properties during multijoint arm posture, Journal of Neuroscience Methods, Vol. 155 , pp. 328-349, 2006

[12] R. Happee, E. de Vlugt, A.C. Schouten, Posture maintenance of the human upper extremity; identification of intrinsic and reflex based contributions, SAE Journal on Passenger Cars and Mechanical Systems, Vol. 1, Issue 1, 2008

[13] A. V. Hill, The heat of shortening and the dynamic constants of muscle. Proc R Soc Lond B, 126:136-195, 1938

[14] P. E. Pfeffer, M. Harrer, D. N. Johnston, Interaction of vehicle and steering system regarding on-centre handling, Vehicle System Dynamics, 46:5,413 — 428, 2008

[15] H. B. Pacejka, Tyre and vehicle dynamics, second edition, Elsevier, 2006

[16] J. P. Switkes, E. J. Rossetter, I. A. Coe and J. C. Gerdes, Handwheel force feedback for lanekeeping assistance: combined dynamics and stability, Journal of Dynamic Systems, Measurement, and Control, 2006

[17] J. M. Carson, W. W. Wierwille, Development of a strategy model of the driver in lane keeping, Vehicle dynamics 7, p. 233-253, 1978

[18] National Highway Traffic Safety Administration (NHTSA) website: www.nhtsa.dot.gov

[19] D. T. McRuer, E. S. Krendel, The human operator as a servo system, Journal of the Franklin Institute, 1959

[20] D. T. McRuer and H. R. Jex, A review of quasi-linear pilot models, IEEE Transactions on human factors in electronics, Vol. 8, No. 3, 1967

[21] D. McRuer, D. H. Weir, Theory of manual vehicular control, IEEE Transactions on Man-Machine Systems, 1969

[22] D. T. McRuer, E. S. Krendel, Mathematical models of human pilot behavior, N.A.T.O. AGARDograph, No. 188, 1974

[23] C. C. MacAdam, Development of a driver model for near/at-limit vehicle handling, UMTRI-2001-43, General Motors, 2001

[24] A. Y. Ungoren, H. Peng, An adaptive lateral preview driver model, Vehicle system dynamics, 2005
[25] D. A. Abbink, Parameter identification of the neuromuscular dynamics of a driver during a relax position task, to be published
[26] M. Kondo, A. Ajimine, Drivers' sight point and dynamics of the driver-vehicle-system related to it, SAE technical paper, 680104, 1968
[27] F. C. T. van der Helm, A. C. Schouten, E. de Vlugt, G. G. Brouwn, Identification of intrinsic and reflexive components of human arm dynamics during postural control, Journal of Neuroscience Methods, 119 1-14, 2002
[28] A.C. Newberry, M. J. Griffin and M. Dowson, Driver perception of steering feel, Proceedings of the Institution of Mechanical Engineers, Part D, Journal of Automobile Engineering, 221, 405-415, 2007
[29] K. K. Tsoi, Development of a haptic feedback transition algorithm for lane changes, Master Thesis TU Delft, 2009
[30] L. A. Rozendaal, Stability of the shoulder. PhD thesis, Delft University of Technology, The Netherlands, 1997
[31] D. T. McRuer, H. R. Jex, A review of quasi-linear pilotmodels, IEEE Transactions on Human Factors, 1967
[32] A. V. Hill, The heat of shortening and the dynamic constants of muscle, Proc R Soc Lond B, 126:136-195, 1938
[33] R. S. Sharp, D. Casanova and P. Symonds, A mathematical model for driver steering control, with design, tuning and performance results. Vehicle System Dynamics, Vol. 33, pp 289-326, 2000
[34] P. C. Cacciabue (Ed.), modelling driver behaviour in automotive environments, Springer, 2007
[35] C. C. Macadam, Understanding and Modeling the Human Driver, Vehicle System Dynamics, Vol. 40 No. 1, pp 101 —134, 2003
[36] M. Plöchl and J. Edelmann, Driver models in automobile dynamics application, Vehicle System Dynamics, Vol. 45, No. 7, pp 699 — 741, 2007
[37] K. Guo, H. Guan, Modelling of Driver/Vehicle Directional Control System, Vehicle System Dynamics, 22:3, p 141 - 184, 1993
[38] I. I. Delice, S. Ertugrul, Intelligent modelling of human driver: a survey, Proc. of the 2007 IEEE Intelligent Vehicles Symposium Istanbul, Turkey, 2007
[39] L. Segel, An investigation of automobile handling as implemented by a variable-steering automobile, Human Factors, Vol. 6, 1964
[40] D. Toffin, G. Reymond, A. Kemeny, J. Droulez, Influence of steering wheel torque feedback in a dynamic driving simulator, Proc. Of the DSC North America, 2003